Neuroscience
Stem Cells and Regenerative Medicine

Base editing of *Ptbp1* in neurons alleviates symptoms in a mouse model of Parkinson's disease

Reviewed Preprint
v2 • December 3, 2024
Revised by authors

Reviewed Preprint
v1 • May 30, 2024

Desirée Böck ✉, **Maria Wilhelm, Jonas Mumenthaler, Daniel Fabio Carpanese, Peter I Kulcsár, Simon d'Aquin, Alessio Cremonesi, Anahita Rassi, Johannes Häberle, Tommaso Patriarchi** ✉, **Gerald Schwank** ✉

Institute of Pharmacology and Toxicology, University of Zurich, Zürich, Switzerland • Division of Clinical Chemistry and Biochemistry, University Children's Hospital Zurich, University of Zurich, Zurich, Switzerland • Division of Metabolism and Children's Research Center, University Children's Hospital Zurich, Zurich, Switzerland • Neuroscience Center Zurich, University of Zurich and ETH Zurich, Zurich, Switzerland

eLife Assessment

This is an **important** study suggesting that neuron-specific loss of function of the RNA splicing factor Ptbp1 in striatal neurons induces dopaminergic markers and alleviates motor defects in a 6-hydroxydopamine (6-OHDA) mouse model of Parkinson's Disease. The evidence supporting the rescue of motor deficits following Ptbp1 manipulation is **solid**, and, while additional characterization of dopaminergic neuronal identity may be required in future studies, these results have clear implications for Parkinson's disease therapeutics. The study also addresses recent controversial literature on cell reprogramming in Parkinson's Disease and will be of interest to researchers with a focus on the application of gene therapy to rescue neurodegeneration.

https://doi.org/10.7554/eLife.97180.2.sa3

Abstract

Parkinson's disease (PD) is a multifactorial disease caused by irreversible progressive loss of dopaminergic neurons (DANs). Recent studies have reported successful conversion of astrocytes into DANs by repressing polypyrimidine tract binding protein 1 (PTBP1), which led to the rescue of motor symptoms in a chemically-induced mouse model of PD. However, several follow-up studies have questioned the validity of this astrocyte to DAN conversion model. In this study, we devised an adenine base editing strategy to downregulate PTBP1 in astrocytes and neurons in a chemically-induced PD mouse model. While PTBP1 downregulation in astrocytes had no effect, we observed that PTBP1 downregulation in neurons of the substantia nigra pars compacta and striatum resulted in the expression of the DAN marker tyrosine hydroxylase (TH) in non-dividing neurons, which was associated with an increase in striatal dopamine concentrations and a rescue of forelimb akinesia and spontaneous rotations. Phenotypic analysis using multiplexed iterative immunofluorescence

imaging further revealed that most of the TH-positive cells in the striatum co-expressed the dopaminergic marker DAT and the pan-neuronal marker NEUN, with the majority of these triple-positive cells being classified as mature GABAergic neurons. Additional research is needed to fully elucidate the molecular mechanisms underlying the expression of the observed markers and understand how the formation of these cells contributes to the rescue of spontaneous motor behaviors. Nevertheless, our findings support a model where neuronal, but not astrocytic, downregulation of PTBP1 can mitigate symptoms in PD mice.

Introduction

Parkinson's disease (PD) is a complex and multifactorial disorder, characterized by the progressive and irreversible loss of dopaminergic neurons (DANs) in the substantia nigra pars compacta (SNc), which leads to the disruption of the nigrostriatal pathway and depletion of striatal dopamine (Bloem et al., 2021; Gitler et al., 2017; Moore et al., 2005). The cause of PD is unknown and only a handful of genetic and environmental risk factors have been identified (Brown et al., 2005; de Lau and Breteler, 2006; Elbaz et al., 2007; Kalia and Lang, 2015), making the development of a curative therapy challenging. In fact, current treatment strategies do not focus on slowing down or halting disease progression, but rather aim to control symptoms and maintain the patients' quality of life (Stoker and Barker, 2020).

Recently emerging *in vivo* transdifferentiation approaches, which leverage the plasticity of specific somatic cell types, hold great promise for developing therapies targeting a wide range of neurodegenerative diseases, including PD (Cohen and Melton, 2011; Torper and Götz, 2017). Astrocytes are of particular interest for such cell fate-switching approaches. First, they are non-neuronal cells and thus not affected by neurodegeneration (Yu et al., 2020). Second, they can acquire certain characteristics of neural stem cells, including multipotency, when activated (Niu et al., 2013; Buffo et al., 2008; Robel et al., 2011; Shimada et al., 2012; Sirko et al., 2013). Finally, they are highly proliferative upon brain injuries such as neurodegeneration (Yu et al., 2021). Several *in vivo* studies have reported successful reprogramming of astrocytes to neurons via overexpression of proneuronal lineage-specific transcription factors, such as NEUROD1 or SOX2 (Guo et al., 2014; Niu et al., 2015, 2013). Moreover, two recent studies have shown that repression of the RNA-binding protein polypyrimidine tract binding protein 1 (PTBP1), which mainly functions as a splicing regulator (Valcárcel and Gebauer, 1997), efficiently converts astrocytes into DANs in the SNc or striatum (Qian et al., 2020; Zhou et al., 2020). Consequently, this led to the restoration of the nigrostriatal pathway and striatal dopamine levels, as well as rescue of motor deficits in a chemically-induced mouse model of PD (Qian et al., 2020; Zhou et al., 2020). However, since the publication of these two studies in 2020, stringent lineage-tracing strategies have revealed that neither quiescent nor reactive astrocytes convert to DANs upon PTBP1 depletion in the SNc or striatum (Chen et al., 2022; Hoang et al., 2023; Wang et al., 2021), fueling widespread debate about the origin of these *de novo* generated cells and their ability to alleviate motor deficits in PD mice (Arenas, 2020; Jiang et al., 2021; Qian et al., 2021).

In this study, we emplyed adenine base editors (ABEs), which enable gene editing independent of DNA double strand break formation (Gaudelli et al., 2017) and thus without the risk of inducing chromosomal rearrangements, translocations, or large deletions (Adikusuma et al., 2018; Kosicki et al., 2018; Shin et al., 2017), to install a loss-of-function splice mutation in the *Ptbp1* gene in astrocytes or neurons. Using a chemically-induced PD mouse model, we show that downregulation of neuronal rather than astroglial PTBP1 in the SNc and striatum improves forelimb akinesia and spontaneous rotations. Histological analysis revealed that downregulation of neuronal PTBP1 induced expression of tyrosine hydroxylase (TH), which is the rate-limiting enzyme in the biosynthesis of dopamine and other catecholamines and thus a characteristic marker of DANs, in

non-dividing neurons of the striatum. Since lack or dysfunction of TH results in dopamine deficiency and parkinsonism, induction of TH expression in striatal neurons may explain the observed rescue of PD phenotypes in mice and provide therapeutic benefits for PD patients.

Results

Adenine base editing effectively downregulates PTBP1 in cell lines

Base editors (BEs) are CRISPR-Cas derived genome engineering tools that allow the precise conversion of A-T to G-C (adenine BEs, ABEs) or C-G to T-A (cytidine BEs, CBEs) base pairs in cell lines as well as post-mitotic cells (Gaudelli et al., 2017; Koblan et al., 2021; Komor et al., 2016; Levy et al., 2020; Villiger et al., 2018). BEs can thus be applied to precisely disrupt canonical splice sites and permanently eliminate gene function *in vivo* (Kluesner et al., 2021; Musunuru et al., 2021; Rothgangl et al., 2021; Winter et al., 2019). To achieve effective and permanent repression of PTBP1, we sought to utilize ABEs to mutate canonical splice sites. To assess if adenine base editing can be used to effectively disrupt PTBP1 expression, we designed seven sgRNAs targeting canonical *Ptbp1* splice donor or acceptor sites in murine Hepa1-6 cells (hereafter referred to as Hepa; **Figure 1 – figure supplement 1**). Plasmids expressing the sgRNAs were co-delivered with *Sp*Cas-, *Sp*G-, or *Sp*Cas-NG-ABE-expressing plasmids into Hepa cells, and genomic DNA was isolated at 5 days post-transfection for analysis by deep sequencing. In line with previous reports (Kluesner et al., 2021), base editing activity was higher at splice donor sites, with the highest editing rates at the exon-intron junctions of exon 3 (92.9±1.0% for *Sp*G-ABE8e) and 7 (85.0±7.2% for *Sp*Cas-ABE8e; **figure 1 – figure supplement 1**). Next, we validated whether both sgRNAs resulted in a reduction of transcript and protein levels. Average editing rates of 77% (sgRNA-ex3) and 73% (sgRNA-ex7) on genomic DNA (**Figure 1 – figure supplement 2**) resulted in approximately 70% and 50% reduction of *Ptbp1* transcripts in Hepa cells (**Figure 1 – figure supplement 2**), leading to a substantial reduction in PTBP1 protein levels and a significant increase in the transcription of exons known to be repressed by PTBP1 (Han et al., 2014; Li et al., 2014) (**Figure 1 – figure supplement 2**).

To analyze whether PTBP1 can also be downregulated by adenine base editing in neuronal and astroglial cells, we repeated experiments with sgRNA-ex3 and the ABE8e-*Sp*G variant in the neuronal Neuro2a and astroglial C8-D1A cell lines (hereafter referred to as N2a and C8-D1A). Compared to Hepa cells (92.9±1.0%; **figure 1 – figure supplement 2**), editing rates were lower in both cell lines (N2a: 64±7.9%; C8-D1A: 62.7±15.1%; **figure 1A**). Nevertheless, we again detected a substantial reduction of *Ptbp1* mRNA and PTBP1 protein levels (**Figure 1B and C**). Notably, editing of the canonical splice donor at exon 3 generated alternative *Ptbp1* splice sites in all three cell lines (**Figure 1 – figure supplement 3**), which, however, did not result in functional PTBP1 protein (**Figure 1C**; **figure 1 – figure supplement 2**). Based on these results, we decided to use sgRNA-ex3 in combination with the *Sp*G-ABE8e variant for *in vivo* experiments.

Downregulation of PTBP1 in neurons of the SNc generates TH-expressing cells

To study the effect of PTBP1 downregulation on an injured nigrostriatal circuit in mice, we first induced a unilateral lesion in the medial forebrain bundle (mfb) using the toxic dopamine analogue 6-hydroxydopamine (6-OHDA; **figure 2 – figure supplement 1**) (da Conceição et al., 2010), similar to previous studies (Chen et al., 2022; Hoang et al., 2023; Qian et al., 2020; Zhou et al., 2020). 5 weeks after the introduction of a lesion, we quantified the loss of TH^+ DANs in the SNc and DA fibers in the striatum by histology (**Figure 2 – figure supplement 1**). As expected, 6-OHDA induced a severe unilateral lesion in the nigrostriatal pathway (**Figure 2 – figure supplement 1**), characterized by an average 99% reduction in the number of TH^+ DANs in the SNc ipsilateral to the injection site (intact hemisphere: 10547±2313 TH^+ cells; lesioned

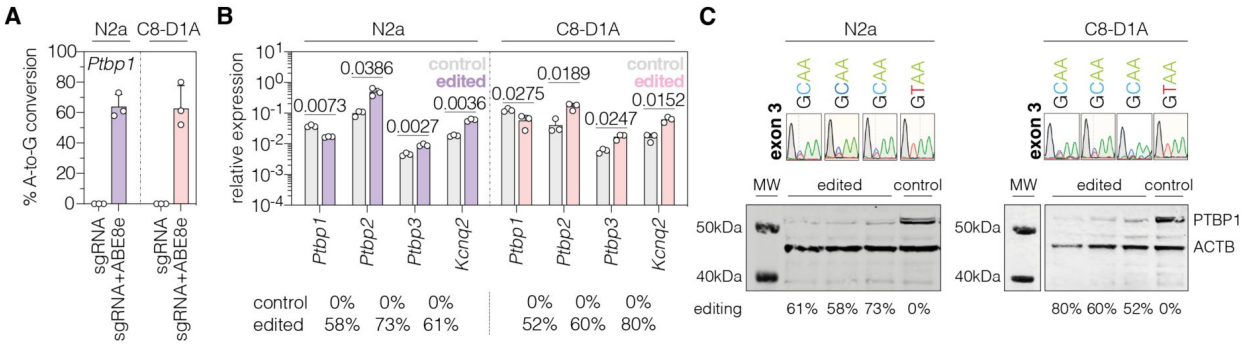

Figure 1

| PTBP1 downregulation by adenine base editing with sgRNA-ex3 in neuronal and astroglial cell lines.

(A) Editing rates at the *Ptbp1* splice donor of exon 3 in N2a and C8-D1A cell lines. Editing efficiencies were determined by Sanger sequencing and EditR (Kluesner et al., 2018). Control samples were transfected with sgRNA (gray). **(B)** Transcript levels of *Ptbp1* and *Ptbp1*-repressed exons upon adenine base editing in N2a and C8-D1A cells. Transcripts were normalized to *Gapdh*. **(C)** PTBP1 levels in control (1 independent experiment) and edited N2a or C8-D1A cells (3 independent experiments). ACTB protein levels are shown as a loading control. Corresponding sequencing chromatograms for sgRNA-ex3 are shown above each sample. Corresponding editing rates are shown below the plots in (B) and (C). Normal distribution of the data was analyzed using the Shapiro-Wilk test. Data are represented as means±s.d. of three independent experiments (A,B) and were analyzed using an unpaired two-tailed Student's t-test with Welch's correction (B). Each datapoint represents one independent experiment. Exact *P*-values are indicated in the respective plots. *Ptbp1*, Polypyrimidine tract binding protein 1; *Ptbp2*, Polypyrimidine tract binding protein 2; *Ptbp3*, Polypyrimidine tract binding protein 3; *Kcnq2*, potassium voltage-gates channel subfamily Q member 2; MW, molecular weight marker; kDa, kilodalton.

hemisphere: 114±83 TH^+ cells; **figure 2 – figure supplement 1**) and an average 92% decrease in fluorescence signal corresponding to striatal DA fibers (dorsal and ventral; **figure 2 – figure supplement 1**). In line with previous reports (Chen et al., 2022), we also observed a sharp increase in activated astrocytes, as indicated by the upregulation of the intermediate filament protein GFAP (glial fibrillary acidic protein; **figure 2 – figure supplement 1**). Finally, we analyzed perturbations in spontaneous motor activities following the 6-OHDA lesion (Boix et al., 2015; Glajch et al., 2012; Iancu et al., 2005) and found that ipsilateral rotations and contralateral forelimb akinesia were significantly increased (**Figure 2 – figure supplement 1**).

In order to target PTBP1 in astrocytes or neurons of 6-OHDA-induced PD mice, we designed adeno-associated virus (AAV) vectors expressing the *Sp*G-ABE8e variant under the control of the astrocyte-specific short GFAP promoter (Lee et al., 2008) (hereafter referred to as AAV-GFAP), or the neuron-specific human synapsin 1 promoter (hsyn) (Kügler et al., 2003) (hereafter referred to as AAV-hsyn). Both vectors additionally express sgRNA-ex3 under the human U6 promoter (Duvoisin et al., 2012). As a non-targeting control, we generated an AAV vector that expresses *Sp*G-ABE8e from the ubiquitous Cbh promoter (Gray et al., 2011), but does not contain sgRNA-ex3 (hereafter referred to as AAV-ctrl). Since ABE8e exceeds the packaging capacity of a single AAV (~5 kb including ITRs) (Grieger and Samulski, 2005), we used the intein-mediated protein trans-splicing system from *Nostoc punctiforme* (*Npu*) (Li et al., 2008; Truong et al., 2015) to split the ABE for expression from two separate AAVs (**Figure 2 – figure supplement 2**). After confirming on-target editing in N2a and C8-D1A cells (**Figure 2 – supplement 2**), we packaged intein-split ABE8e expression vectors into AAV-PHP.eB capsids and delivered particles to the SNc of C57BL/6J mice 5 weeks after the introduction of the unilateral 6-OHDA lesion (**Figure 2A**). 12 weeks after AAV treatment at a dose of $2ξ10^8$ vector genomes (vg) per animal, we assessed whether the injured nigrostriatal pathway was reconstituted (**Figure 2A**).

When we first analyzed animals treated with AAV-ctrl, we observed an average 99% reduction of TH^+ cells in the SNc of lesioned animals (intact hemisphere: 8678±2765 TH^+ cells; lesioned hemisphere: 122±26 TH^+ cells; **Figure 2B and C**). When we next assessed animals treated with AAV-hsyn to downregulate PTBP1 in neurons, we observed a restoration of approximately 10% of TH^+ cells compared to the intact hemisphere (intact hemisphere: 7613±1386 TH^+ cells; lesioned hemisphere: 721±144 TH^+ cells; **Figure 2B and D**). In contrast, when we analyzed animals treated with AAV-GFAP to downregulate PTBP1 in astrocytes, we did not observe TH^+ cells above control levels (intact hemisphere: 9209±1199 TH^+ cells; lesioned hemisphere: 158±78 TH^+ cells; **figure 2C and D**; **figure 2 – figure supplement 3**). However, despite the presence of TH+ cells in the SNc of AAV-hsyn-treated animals, we did not detect an increase in fluorescence signal corresponding to DA fibers in the striatum, suggesting that TH^+ cells generated in the SNc upon neuronal PTBP1 downregulation did not form striatal projections (**Figure 2E and F**). Further supporting this observation, we did not detect differences in fluorescence intensity between groups when analyzing projections of DANs in the mfb (**Figure 2 – figure supplement 4**). Notably, base editing at the *Ptbp1* splice site (AAV-ctrl, 0.04±0.03%, AAV-GFAP, 14.7±3.9%; AAV-hsyn, 15.5±8.5%) as well as a reduction of *Ptbp1* transcript (AAV-GFAP, 23.7±12.7%; AAV-hsyn, 24.8±18.7%) and PTBP1 protein levels (AAV-GFAP, 10.8±6.3%; AAV-hsyn, 13.8±10.1%) could be confirmed in SNc tissues at experimental endpoints (**Figure 2 – figure supplement 5**).

Taken together, our results suggest that PTBP1 downregulation in neurons of the SNc generates TH^+ cells; however, unlike endogenous DANs in the SNc, they do not project to the dorsal striatum.

Downregulation of PTBP1 in neurons of the striatum generates TH^+ cells and increases striatal dopamine levels

Since the observed TH^+ cells in the SNc did not generate projections to reconstruct the nigrostriatal pathway, we next tested whether we could bypass the lack of striatal projections by generating TH^+ cells directly in the striatum. We therefore delivered AAV-hsyn at a dose of $4ξ10^8$

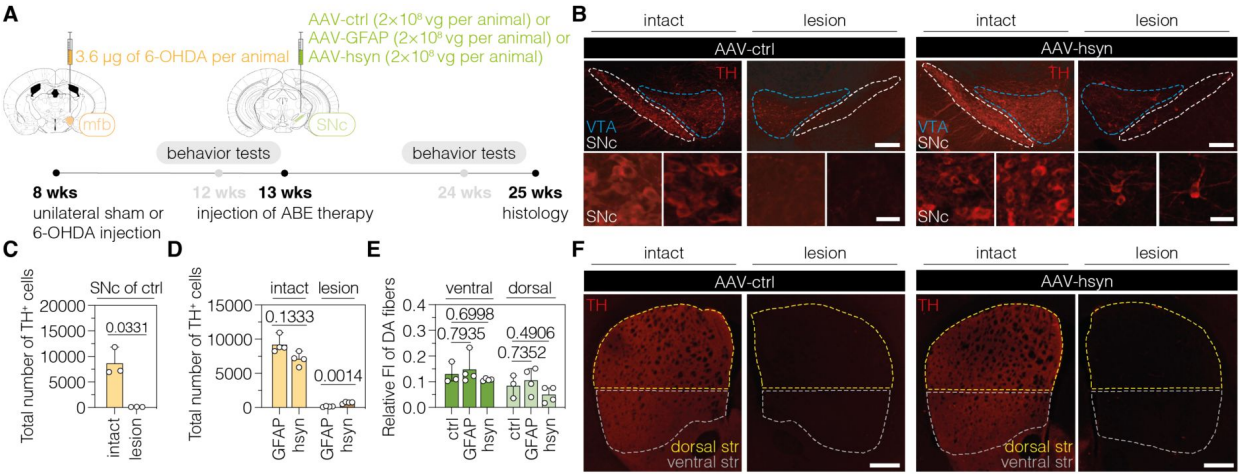

Figure 2

| Downregulation of PTBP1 in neurons of the SNc generates TH$^+$ cells.

(A) Schematic representation of the experimental timeline and setup. **(B)** Representative images of midbrain sections showing the intact (left) or lesioned (right) SNc in animals treated with AAV-ctrl (left) or AAV-hsyn (right). Treatment groups and hemispheres are indicated on top. **(C,D)** Quantification of TH$^+$ cells in the intact or lesioned SNc in animals treated with AAV-ctrl (C), AAV-GFAP (D), or AAV-hsyn (D) in the lesioned hemisphere. **(E,F)** Quantifications (E) of DA fibers in the striatum, assessed as relative fluorescence intensity (FI) of TH compared to the intact striatum of the same section, and representative images of brain sections (F) showing the intact or denervated striatum (str) in animals treated with AAV-ctrl (left) or AAV-hsyn (right). The FI of the TH staining detected in the corpus callosum of each hemisphere was used for background correction of FI detected in the striatum of the same hemisphere. Control animals were treated with AAV-PHP.eB particles, expressing the ABE8e variant under the ubiquitous Cbh promoter. Tissue areas used for quantifications are marked by colored dashed lines in (B) and (E). Normal distribution of the data was analyzed using the Shapiro-Wilk test. Data are represented as means±s.d. of 3-8 animals per group and were analyzed using an unpaired two-tailed Student's t-test with Welch's correction (C, D) or a one-way ANOVA with Dunnett's multiple comparisons test (E). Each datapoint represents one animal. Exact *P*-values are indicated in the respective plots. Scale bars, 20 µm (B, bottom) and 1000 µm (B, top; F). ctrl, AAV-ctrl-ABE treatment; GFAP, AAV-GFAP-ABE treatment; hsyn, AAV-hsyn-ABE treatment; ABE, adenine base editor; vg, vector genomes; SNc, substantia nigra pars compacta; VTA, ventral tegmental area; TH, tyrosine hydroxylase; str, striatum; FI, fluorescence intensity; DA, dopaminergic.

vg per animal into the striatum of C57BL/6J mice, which were pre-treated with 6-OHDA to generate a unilateral lesion. The injection volume, and thus the delivered AAV dose, was increased compared to the SNc to achieve comparable AAV biodistribution in the larger striatum. Confirming the unilateral impairment of the nigrostriatal pathway, analysis of brain sections at 12 weeks post-treatment revealed an average 99% reduction of TH^+ cells in the lesioned SNc and no detectable DA projections to the striatum (**Figure 3 – figure supplement 1**). When we quantified TH^+ cells in brain sections of the striatum, we found 106±38 TH^+ cells across 3 sections (estimated as 2646±952 cells in the entire striatum) in mice treated with AAV-hsyn compared to no TH^+ cells in the lesioned hemisphere of animals treated with AAV-ctrl (**Figure 3A**). Analysis of striatum tissues isolated from AAV-ctrl– and AAV-hsyn-treated PD mice revealed base editing at the *Ptbp1* splice site (AAV-ctrl, 0.4±0.1%; AAV-hsyn, 23.0±6.6%; **Figure 3 – figure supplement 2**) and downregulation of *Ptbp1* transcript (AAV-hsyn, 30.8±14.6%) and PTBP1 protein levels (AAV-hsyn, 22.1±6.4%; **figure 3 – supplement 2**).

Since we did not observe PTBP1 downregulation or TH^+ cells in animals treated with AAV-ctrl (**Figure 3A**; **figure 3 – figure supplement 2**), we can rule out that TH expression is induced by 1) tissue damage due to the injection procedure or 2) toxicity due to the administered AAV dose or serotype. To additionally exclude that TH expression might be caused by off-target editing effects, we experimentally determined off-target sites of sgRNA-ex3 using GUIDE-seq in N2a cells (Tsai et al., 2014) and subsequently analyzed these sites in treated animals by deep amplicon sequencing (**Figure 3 – supplement 3**). One off-target site was identified in the myopalladin (*Mypn*) gene, which encodes for a muscle-specific protein and plays a critical role in regulating the structure and growth of skeletal and cardiac muscle (Filomena et al., 2021, 2020), and another site was detected in the intronic region of the ankyrin-1 (*Ank1*) gene, which encodes for an adaptor protein linking membrane proteins to the underlying cytoskeleton (Cunha and Mohler, 2009). Importantly, base editing rates at both sites were substantially lower (*Mypn*, 5.4±1.7%; *Ank1*, 5.8±1.9%; **Figure 3 – figure supplement 3**) than at the *Ptbp1* site in AAV-hsyn-treated mice (23.0±6.6%; **Figure 3 – figure supplement 2**) and no reduction in transcript levels of the respective genes was observed (**Figure 3 – figure supplement 3**). Thus, the induction of TH expression upon adenine base editing with sgRNA-ex3 is likely a direct consequence of PTBP1 downregulation.

Next, we assessed whether the ectopic expression of TH in the striatum led to an increase in tissue dopamine levels. We manually dissected striata of lesioned and unlesioned hemispheres and quantified tissue dopamine levels by high-pressure liquid chromatography (HPLC; **figure 3 – figure supplement 4**). Peak identities and neurotransmitter concentrations were analyzed using corresponding standards of known concentrations. Importantly, base edited animals showed an approximately 2.5-fold increase in the concentration of striatal dopamine (AAV-hsyn: 4.4±2.6 nmol/g protein; AAV-ctrl: 1.7±0.7 nmol/g protein) and the dopamine metabolite 3,4-dihydroxyphenylacetic acid (DOPAC; AAV-hsyn: 8.2±3.9 nmol/g protein; AAV-ctrl: 3.1±1.8 nmol/g protein) in the lesioned hemisphere (**figure 3 – figure supplement 4**).

Taken together, our data suggest that downregulation of PTBP1 in striatal neurons of 6-OHDA-lesioned hemispheres resulted in the expression of TH and an elevation of striatal dopamine concentrations.

Phenotypic characterization of TH^+ cells in the striatum

To characterize the TH-expressing cells in the SNc and striatum of AAV-hsyn-treated mice in more detail, we co-stained them for the pan-neuronal marker NEUN (hexaribonucleotide binding protein-3). As expected, virtually all TH^+ cells in the intact SNc were co-stained for NEUN (99.0±0.1%; **figure 3B**). Likewise, the majority of TH^+ cells in the lesioned SNc (hsyn: 92.0±6.2%; **figure 3B**) and striatum of AAV-hsyn-treated animals (77.5±11.8%; **figure 3C**) were also labelled by NEUN, further corroborating a neuronal origin of these cells. Moreover, we observed a

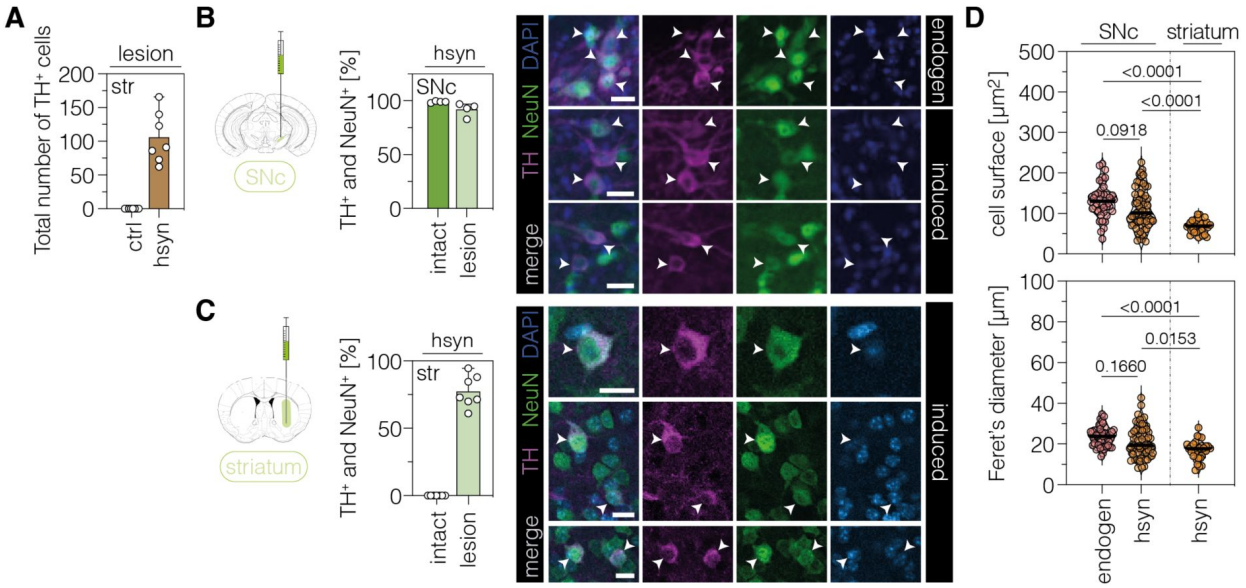

Figure 3

| Characterization of TH-expressing cells in the SNc or striatum.

(A) Quantification of TH^+ cells in the lesioned striatum of animals treated with AAV-ctrl or AAV-hsyn. Control animals were treated with AAV-PHP.eB particles, expressing the ABE8e-*Sp*G variant under the ubiquitous Cbh promoter. **(B,C)** Quantifications (left) and representative images (right) of TH/NeuN double-positive cell bodies in the intact (dark green, labelled as "endogen" in the images) or lesioned (light green, labelled as "induced" in the images) SNc (B) or striatum (C) of AAV-hsyn-treated animals. **(D)** Corresponding quantifications of cell surface area and Feret's diameter (longest distance between the cell boundaries) of TH/NeuN double-positive cell bodies in the intact (labeled as "endogen") or lesioned SNc or striatum (labeled as "hsyn"). Normal distribution of the data was analyzed using the Shapiro-Wilk test. Data are displayed as means±s.d. of 4-7 mice per group (A-C) or 32-68 TH/NeuN double-positive cells per group (D; n=4 mice) and were analyzed using a one-way ANOVA with Tukey's multiple comparisons test (D). Each datapoint represents one animal (A-C) or a TH/NeuN double-positive cell (D). Exact *P*-values are indicated in the each plot above the respective group (D). Scale bars, 20 µm. ctrl, AAV-ctrl-ABE treatment; hsyn, AAV-hsyn-ABE treatment; SNc, substantia nigra pars compacta; str, striatum; TH, tyrosine hydroxylase; NEUN, hexaribonucleotide binding protein-3; DAPI, 4',6-diamidino-2-phenylindole; endogen, endogenous.

significant reduction in the surface area and Feret's diameter between TH/NEUN double-positive cells in the lesioned striatum compared to endogenous DANs in the intact SNc, or TH/NEUN double-positive cell bodies in the lesioned SNc of AAV-hsyn-treated mice (**Figure 3D**).

Differences in the frequency of NEUN-labeling, as well as surface area and diameter of TH^+ cells in the striatum might be attributed to 1) varying maturation states of these cells, potentially influenced by the local microenvironment of the SNc vs striatum, and/or 2) TH-expressing cells originating from distinct neuronal subpopulations. In line with previous work (Qian et al., 2020), injection of AAV-hsyn into the visual cortex did not lead to TH expression in local neurons (**Figure 3 – figure supplement 5**; n=174 Cas9/NEUN double-positive cells), suggesting that the local microenvironment indeed plays a contributing role in inducing TH expression in the targeted neurons. To next analyze the origin of TH-expressing cells in the striatum, we first assessed whether these cells originated from dividing neural progenitors or mature, non-dividing neurons. We therefore supplied bromodeoxyuridine (BrdU)-containing drinking water to 6-OHDA-lesioned mice after AAV-hsyn treatment (**Figure 3 – figure supplement 6**). After confirming successful BrdU labeling of proliferating cells in the dentate gyrus (DG; **figure 3 – figure supplement 6**), we performed BrdU/NEUN/TH co-staining experiments with striatal sections. Microscopic analysis of 163 TH/NEUN double-positive cells revealed no co-labeling with BrdU (**Figure 3 – figure supplement 6**), indicating that TH^+ cells were not generated *de novo* and rather originated from non-proliferating mature neurons.

Next, we performed multiplexed iterative immunofluorescence imaging (4i) (Cole et al., 2022) on tissue sections to further characterize the identity, origin, and differentiation state of these cells (**Figure 4**). After successful validation of antibody specificities (**Figure 4 – supplement 1**), we performed four 4i rounds using markers for neural progenitors (SOX2/sex determining region Y-box 2, NES/neuroepithelial stem cell protein, DCX/doublecortin), DANs (TH, DAT), and mature neurons (NEUN, CTIP2/COUP-TF-interacting protein 2, SST/somatostatin, PV/parvalbumin, CALB2/calbindin 2). The majority of TH^+ cells also expressed the marker DAT (75.2±5.6%; **figure 4A**, B), further corroborating the DA identity of these cells. Moreover, supporting the results of our BrdU-labeling experiments (**Figure 3 – figure supplement 6**), only a small fraction of TH/DAT double-positive cells were labeled for markers of neural progenitors (SOX2, 9.1±2.4%; NESTIN, 2.1±0.5%; DCX, 2.6±0.8%; **figure 4A**, B). Instead, most TH/DAT-labeled cells expressed the adult pan-neuronal marker NEUN (86.2±3.7%; **figure 4A**, B). Of this TH/DAT/NEUN-positive population, 49.8±12.9% were additionally labeled with CTIP2 (**Figure 4A** and **4B**), a marker for GABAergic medium spiny neurons (MSNs), and 46.4±10.4% expressed markers for various GABAergic interneurons (PV, 3.2±1.9%; SST, 3.5±1.2%; CALB2, 39.7±11.0%; **figure 4A** and 4B), indicating that expression of DA markers may be achieved in various subtypes of GABAergic neurons upon PTBP1 downregulation.

In summary, our data show that TH-expressing cells were not generated from proliferating neural stem cells, but rather originated from various populations of post-mitotic striatal neurons that acquired DA characteristics upon PTBP1 downregulation.

Neuronal PTBP1 repression alleviates drug-free motor dysfunction in PD mice

Last, we evaluated whether neuronal and/or astroglial base editing of PTBP1 in the SNc and/or striatum could restore motor functions in mice with a unilateral 6-OHDA lesion. We first performed two common drug-free behavioral tests: the cylinder test to quantify the asymmetry of spontaneous rotations and the stepping test to quantify contralateral forelimb akinesia (Boix et al., 2015; Glajch et al., 2012; Iancu et al., 2005). We found that drug-free motor dysfunctions were significantly alleviated in animals treated with AAV-hsyn, but not with AAV-GFAP, in the SNc when using an AAV dose of $2\xi10^8$ vg per animal (**Figure 5 – figure supplement 1**). Likewise, PTBP1 targeting in striatal neurons restored the asymmetry of spontaneous behaviors (**Figure**

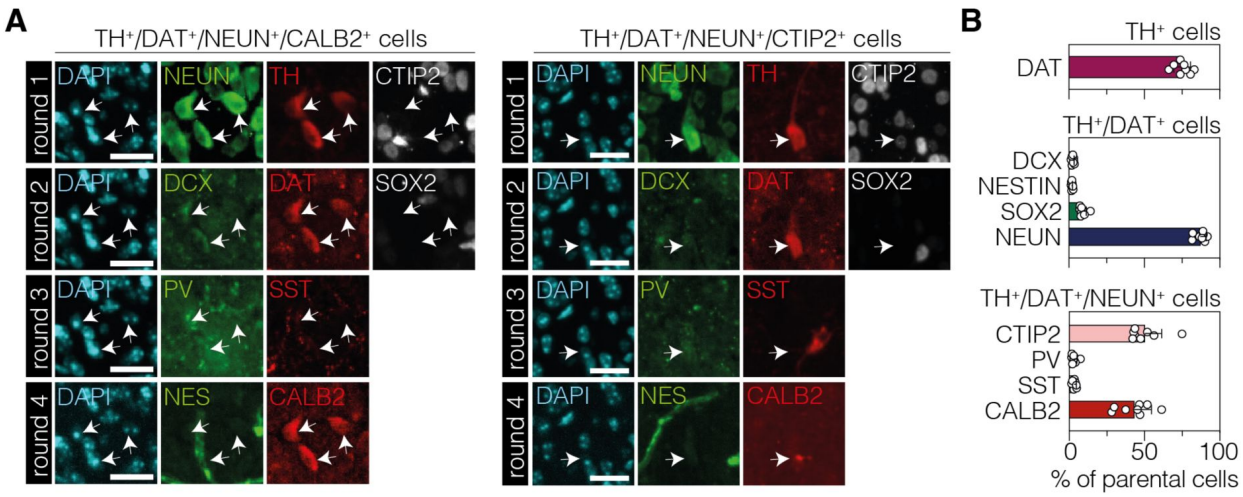

Figure 4

| Characterization of TH$^+$ cells in the striatum after neuronal PTBP1 downregulation.

(**A**) Representative 4i images of the two main cell populations among TH-positive cells. The expressed markers are indicated on top of the images. (**B**) Corresponding quantifications of phenotypic markers expressed among TH-positive cells (top, DAT; n=696 TH$^+$ cells), TH/DAT double-positive (middle, DCX; NESTIN; SOX2; n=527 cells), or TH/DAT/NEUN triple-positive (bottom, CTIP2; PV; SST; CALB2; n=460 cells) subpopulations (white arrows) in the striatum at 12 weeks after administration of the AAV-hsyn treatment. The parental population is indicated above each plot. 4i imaging rounds are indicated on the left in (A). Images were pseudocolored during post-processing. Scale bars, 20µm. Data are displayed as means of 6 mice (B). DAPI, 4',6-diamidino-2-phenylindole; SOX2, sex determining region Y-box 2; NES, neuroepithelial stem cell protein; DCX, doublecortin; NEUN, hexaribonucleotide binding protein-3; TH, tyrosine hydroxylase; DAT, dopamine transporter; CTIP2, COUP-TF-interacting protein 2; PV, parvalbumin; SST, somatostatin; CALB2, calbindin 2.

5A and **5B**). To assess the extent of motor improvements in response to the ABE treatment, we additionally tested two drug-induced motor behaviors. However, we did not detect recovery of contralateral rotations in treated animals after systemic administration of amphetamine (**Figure 5C**; **figure 5 – figure supplement 1**), which leads to an enhanced imbalance of extracellular dopamine concentrations between the denervated and intact striatum (Freyberg et al., 2016; Karam et al., 2022). Likewise, after systemic administration of apomorphine, which acts as a dopamine receptor agonist and stimulates hypersensitive dopamine receptors in the lesioned hemisphere (Arroyo-García et al., 2018; da Conceição et al., 2010; Iancu et al., 2005), we did not observe a recovery of ipsilateral rotations in any treatment group (**Figure 5D**; **figure 5 – figure supplement 1**).

Taken together, downregulation of PTBP1 in SNc and striatal neurons improves spontaneous, but not drug-induced, behaviors in 6-OHDA-lesioned mice.

Discussion

In this study, we applied adenine base editing to introduce *Ptbp1* loss-of-function mutations in astrocytes and neurons in the 6-OHDA-induced PD mouse model. Delivery of dual AAV vectors to the SNc resulted in the formation of TH-expressing cells and rescue of spontaneous behaviors when a neuronal promoter was used to drive ABE expression. However, no DA projections to the striatum were detected, supporting recent findings that suggest a functional role of PTBP1 in promoting axon regeneration of adult sensory neurons (Alber et al., 2023). Reconstitution of the nigrostriatal pathway, which connects the SNc with the dorsal striatum (Kalia and Lang, 2015), is therefore unlikely the mechanism underlying the observed phenotypic rescue. Supporting this hypothesis, downregulation of neuronal PTBP1 in the striatum of 6-OHDA-lesioned mice also led to the formation of TH^+ cells and a rescue of spontaneous behaviors.

Two previous studies suggested that PTBP1 downregulation in the SNc, using either shRNA-mediated knockdown or knockdown via CRISPR-CasRx, led to the conversion of astrocytes into functional DANs in 6-OHDA-lesioned mice (Qian et al., 2020; Zhou et al., 2020). However, recent lineage tracing studies revealed that neither quiescent nor reactive astrocytes in the SNc or striatum convert to DANs upon PTBP1 downregulation (Chen et al., 2022; Hoang et al., 2023; Wang et al., 2021). Instead, these studies hypothesize that the reported effects might be attributed to leaky activation of the GFAP promoter in neurons, which could have been misinterpreted as astrocyte to neuron conversion. Our study contributes to this recently growing body of evidence, indicating that downregulation of astroglial PTBP1 does not induce astrocyte conversion into DANs, and that neurons are the origin of the observed TH^+ cells (Chen et al., 2022; Wang et al., 2021; Yang et al., 2023). Our 4i and BrdU experiments furthermore revealed that TH expression in the striatum was induced in mature neurons, either expressing markers of GABAergic MSNs or interneurons. These findings indicate that the induction of TH expression is not restricted to a specific neuronal subpopulation, but may rather be attributed to 1) potential bias of hsyn promoter activity towards inhibitory neurons (Radhiyanti et al., 2021), 2) preferential AAV tropism towards distinct neuronal subpopulations in the striatum, or 3) differences in the local microenvironment, chemical signals, and neuronal circuitry required to induce TH expression in distinct neuronal subpopulations.

While our study suggests that PTBP1 downregulation can enable TH expression in various GABAergic neuronal populations in the striatum, the transcriptional changes leading to and following TH expression in these cells remain unclear. Previous research has demonstrated that the interplay between microRNAs (miRNAs) and the RNA processing proteins PTBP1 and its homology nPTBP (PTBP2) is crucial during neuronal differentiation and maturation (**Fig. 5 – figure supplement 2**) (Boutz et al., 2007; Makeyev et al., 2007; Zheng et al., 2012). Key events in this signaling cascade are the dynamic release of PTBP1-mediated inhibition of miRNA-124, which

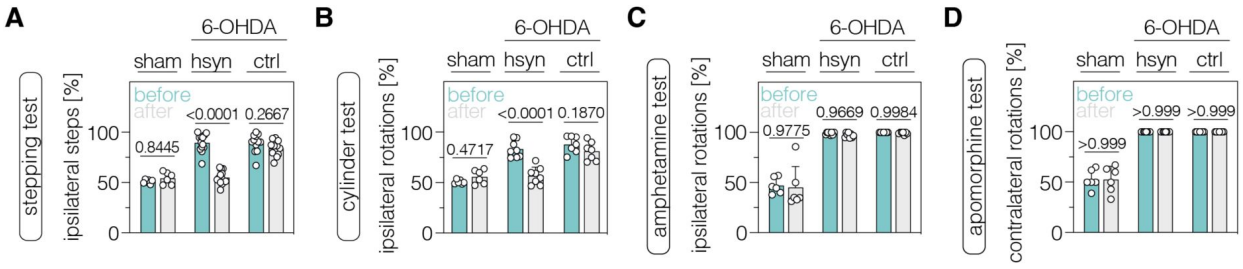

Figure 5

| Neuronal PTBP1 downregulation in the striatum alleviates drug-free motor dysfunction in 6-OHDA-lesioned PD mice. (A,B)

Spontaneous behaviors, assessed as contralateral forelimb akinesia in the stepping test (A) and spontaneous rotations in the cylinder test (B), in animals treated in the striatum. (**C,D**) Drug-induced rotations, assessed as amphetamine-induced ipsilateral rotations (C) and apomorphine-induced contralateral rotations (D), in animals treated in the striatum. Normal distribution of the data was analyzed using the Shapiro-Wilk test. Data are represented as means±s.d. of 6-13 animals per group and were analyzed using a two-way ANOVA with Šidák's multiple comparisons. Each datapoint represents one animal. Exact *P*-values are indicated in each plot. hsyn, AAV-hsyn-ABE treatment; ctrl, AAV-ctrl-ABE treatment.

induces nPTBP expression and activates neuron-specific expression programs in non-neuronal cells (Makeyev et al., 2007; Xue et al., 2013). Thus, the activation of the PTBP1/nPTBP regulatory loops is essential for driving reprogramming towards the neuronal lineage and subsequent neuronal maturation (Xue et al., 2016, 2013). While this classical model of PTBP1 down-regulation and neuronal differentiation implies neglible expression or importance of PTBP1 in mature neurons, our results indicate that PTBP1 is sufficiently expressed and plays a functional role in mature neurons, with the installation of a loss-of-function mutation resulting in detectable reduction in relative protein amounts (**Figure 2 – supplement 5**; **figure 3 – supplement 2**) and behavioral improvements in a PD mouse model (**Figure 5**; **figure 5 – supplement 1**). Supporting these findings, a recent study demonstrated PTBP1 expression in axons of sensory and motor neurons as well as a functional role in sensation, injury response, and axonal regeneration (Alber et al., 2023). Further investigation using single cell transcriptional analysis of the PTBP1/nPTBP regulatory loops, pro-neuronal transcription factors (*Ascl1*, *Myt1l*, *Zic1*, *Brn2*, *NeuroD1*) (Xue et al., 2013), or transcription factors guiding the differentiation into DANs (*Nr4a2*, *LMx1a*, *LMx1b*, or *Pitx3* (Niu et al., 2021)) could provide insights into the transcriptional switches underlying TH expression in MSNs and interneurons as observed in our study.

MSNs, the principal neurons of the striatum (~95%), can be divided into two distinct subtypes based on their expression of dopamine receptors and their axonal projections (D1-or D2-MSNs) (Gerfen et al., 1990; Smith et al., 1998). Both the input to and output from D1– and D2-MSNs are dynamically controlled by striatal interneurons, which constitute approximately 5% of total striatal neurons (Clarke and Adermark, 2015). Since both MSNs and interneurons receive DA inputs from the SNc, their activity and excitability are strongly hampered when striatal dopamine is absent (Bamford et al., 2018; Gerfen and Surmeier, 2011; Kreitzer and Malenka, 2008). It therefore seems feasible that PTBP1 downregulation by adenine base editing and subsequent TH expression might have enabled local dopamine synthesis in the dorsal striatum, which may have been sufficient to partly restore the function of these cell populations and compensate for the depletion of DA inputs from the SNc. Supporting this hypothesis, a recent study has shown that depletion of the orphan G-protein coupled receptor 6 (GPR6) in D2-MSNs reduced intracellular cyclic adenosine monophosphate (cAMP) concentrations, leading to increased striatal dopamine and decreased involuntary movements following apomorphine treatment in 6-OHDA-lesioned PD mice (Sun et al., 2021). When we quantified dopamine levels in the striatum of AAV-hsyn-treated PD mice using HPLC, we observed a 2.5-fold increase in striatal dopamine, suggesting that induction of TH expression in striatal neurons might establish a basal tone of extracellular dopamine despite the absence of striatal DA projections, akin to pharmacological replenishment in PD patients (Poewe et al., 2017). While the increase in dopamine levels was modest compared to 6-OHDA-lesioned rats treated with the dopamine precursor L-DOPA, which exhibited an increase in extracellular dopamine concentrations from ~0.04 fmol/µL to ~9-10 fmol/µL (Lindgren et al., 2010), our results indicate that even a modest increase in striatal dopamine is sufficient to rescue spontaneous motor behaviors in PD mice. This finding aligns with recent work showing that multiple unconditioned DA-dependent motor tasks can be sustained through a diffuse basal tone of extracellular dopamine in the striatum (Delignat-Lavaud et al., 2023). Conversely, basal dopamine levels were insufficient to improve amphetamine-induced behaviors in AAV-hsyn-treated PD mice in this study, potentially due to the lack of striatal projections from the SNc and/or insufficient availability of intracellular dopamine in striatal neurons. Likewise, the detected dopamine levels in striatal tissues were not sufficient to reverse the hypersensitivity of D1 and D2 receptors to the dopamine agonist apomorphine. Higher base editing rates, achievable using either single AAV delivery of smaller Cas9 orthologues or multiple injections into the rostral, medial, and caudal regions of the striatum, may result in more pronounced global PTBP1 downregulation and potentially higher tissue dopamine concentrations, leading to a broader behavioral rescue. Moreover, further analysis using fiber photometry or microdialysis could provide information on synaptic dopamine release and availability.

Transcriptional reprogramming is fundamental for neuronal differentiation and maturation, relying on various feedback and feed-forward circuits to regulate cell type-specific gene expression programs. While loss of PTBP1 is considered crucial for reducing neuronal apoptosis and inducing neuronal differentiation during development, its various roles in mature neurons during adulthood remains largely elusive. Further investigation using single cell transcriptional analysis or spatial transcriptomics is needed to identify the transcriptional changes driving the expression of DA markers in striatal GABAergic neurons upon PTBP1 downregulation. These experiments may also contribute to our understanding of how PTBP1 downregulation may affect cAMP metabolism, dopamine synthesis, and basal ganglia circuitry in PD mice. Finally, to fully explore the therapeutic potential of PTBP1 base editing, future studies should also combine detailed transcriptional analysis with stringent lineage-tracing technologies and *in vivo* assessment of synaptic dopamine availability and release in more sophisticated PD mouse models that exhibit neuropathological, motor, and cognitive aspects of the disease.

Materials and methods

Generation of plasmids

sgRNA plasmids were generated by ligating annealed and phosphorylated oligos into a BsmBI-digested lentiGuide-Puro (Addgene #52963) using T4 DNA ligase (NEB). To generate intein-split ABE plasmids for AAV production, inserts with homology overhangs were either ordered as gBlocks (IDT) or generated by PCR. Inserts were cloned into KpnI– and AgeI-digested AAV backbones using HiFi DNA Assembly Master Mix (NEB). All PCRs were performed using Q5 High-Fidelity DNA Polymerase (NEB). All plasmids were transformed into *Escherichia coli* Stable3 competent cells (NEB). The identity of all plasmids was confirmed by Sanger Sequencing. Primers used for cloning of all plasmids are listed in supplementary tables 1 and 2. LentiGuide-Puro was a gift from F. Zhang (Addgene plasmid nos. 52963).

Cell culture transfection and genomic DNA preparation

Hepa1-6 (ATCC CRL-1830) cells were maintained in Dulbecco's modified Eagle's medium (DMEM) plus GlutaMAX (Thermo Fisher Scientific), supplemented with 10% (v/v) fetal bovine serum (FBS) and 1% penicillin/streptomycin (Thermo Fisher Scientific) at 37°C and 5% CO_2. Neuro2a (ATCC CCL-131) cells were maintained in Eagle's Minimum Essential Medium (EMEM), supplemented with 10% (v/v) FBS and 1% penicillin/streptomycin. C8-D1A [astrocyte type I clone, ATCC CRL-2541] were maintained in Dulbecco's modified Eagle's medium (DMEM) supplemented with 10% (v/v) fetal bovine serum (FBS) and 1% penicillin/streptomycin (Thermo Fisher Scientific) at 37°C and 5% CO_2. Cells were passaged every 3 to 4 days and maintained at confluency below 90%.

For the *in vitro* screening of sgRNA activities, cells were seeded in 96-well cell culture plates (Greiner) and transfected at 70% confluency using 0.5µl Lipofectamine^{TM} 2000 (Thermo Fisher Scientific). If not stated otherwise, 300ng of BE and 100ng of sgRNA were used for transfections. Cells were incubated for 5 days after transfection and genomic DNA was isolated using a direct lysis as previously described (Böck et al., 2022). For analysis of transcript and protein levels, cells were seeded in a 48-well cell culture plate (Greiner) and transfected at 70% confluency using 1µl of Lipofectamine^{TM} 2000 (Thermo Fisher Scientific). A small aliquot of the cells was used for isolation of genomic DNA by direct lysis as previously described (Böck et al., 2022). The remaining cells were split in half for RNA and protein isolation.

For the assessment of *in vivo* base editing performance, a 40 µm thick section of the SNc or striatum was used for manual dissection of these regions under a stereomicroscope. DNA was subsequently isolated from tissue pieces by direct lysis as previously described (Böck et al., 2022).

RNA isolation and RT-qPCR

RNA was isolated from cultured cells or snap-frozen brain tissues (striatum or SNc) using the RNeasy Mini Kit (Qiagen) or the AllPrep DNA/RNA/Protein Mini Kit (Qiagen) according to the manufacturer's instructions. RNA (1000ng input) was subsequently reverse-transcribed to cDNA using random primers and the GoScript reverse transcriptase kit (Promega). RT-qPCR was performed using FIREPolymerase qPCR Master Mix (Solis BioDyne) and analyzed using a Lightcycler 480 system (Roche). Fold changes were calculated using the double ΔCt method. Primers used for RT-qPCR are listed in supplementary table 3.

Protein isolation and western blot

Protein was isolated from cultured cells or snap-frozen brain tissues (striatum or SNc) using radioimmunoprecipitation (RIPA) assay buffer (150 mM Tris pH 8.0, 150 mM NaCl, 0.1% SDS, 0.5% sodium deoxycholate, 1% NP-40; Thermo Fisher Scientific), supplemented with protease inhibitor cocktail (Roche), or the AllPrep DNA/RNA/Protein Mini Kit (Qiagen) according to the manufacturer's instructions. Protein concentrations of all samples were determined using the Pierce Bicinchoninic Acid (BCA) Protein Assay Kit (Thermo Fisher Scientific).

Equal amounts of protein (*in vitro* samples: 30 µg; *in vivo* samples: 40 µg) were separated by SDS-polyacrylamide gel electrophoresis (Thermo Fisher Scientific) and transferred to a 0.45-µm nitrocellulose membrane (Amersham). Membranes were incubated with rabbit anti-PTBP1 (1:10,000; cat. no. ab133734, Abcam) and mouse anti-actin beta (1:2,000; cat. no. ab8226; Abcam). Signals were detected by fluorescence using IRDye-conjugated secondary antibodies (LI-COR Biosciences) and a LICOR Odyssey ® DLx imaging system. Protein quantifications were performed in Fiji. All antibodies are listed in supplementary table 4.

Amplification for deep sequencing

PTBP1-specific oligos were used to generate targeted amplicons for deep sequencing. Input genomic DNA was first amplified in a 10µL reaction for 30 cycles using NEBNext High-Fidelity 2ξPCR Master Mix (NEB). Amplicons were purified using AMPure XP beads (Beckman Coulter) and subsequently amplified for eight cycles using oligos with sequencing adapters. Approximately equal amounts of PCR products were pooled, gel purified, and quantified using a Qubit 3.0 fluorometer and the dsDNA HS Assay Kit (Thermo Fisher Scientific). Paired-end sequencing of purified libraries was performed on an Illumina Miseq platform. Oligos for deep sequencing are listed in supplementary table 5.

HTS data analysis

Sequencing reads were first demultiplexed using the Miseq Reporter (Illumina). Next, amplicon sequences were aligned to their reference sequences using CRISPResso2 (Clement et al., 2019). Adenine base editing efficiencies at splice sites were calculated as percentage of (number of reads containing edits at splice site)/(number of total aligned reads). Reference nucleotide sequences are listed in supplementary table 6.

GUIDE-seq off-target analysis

Briefly, $6ξ10^4$ N2a cells were plated in a 24-well plate one day prior to transfection. Cells were transfected using Lipofectamine 3000 according to the manufacturer's instructions. Three plasmids, encoding for the *Sp*G Cas9 nuclease [333 ng], the *Ptbp1* sgRNA-3 [167 ng], and GFP [6 ng], were co-transfected with 12 pmol of the double-stranded oligodeoxynucleotide (dsODN) following the the original GUIDE-seq protocol (Tsai et al., 2014). Transfections were performed in triplicates. dsODN was transfected as a negative control. Cells were harvested ~96 h post-transfection and genomic DNA was purified. Efficient indel formation at the on-target site and

integration of the dsODN tag were confirmed through deep amplicon sequencing. Genomic DNA was subsequently sheared with Covaris E220 to on average 500 bp according to the manufacturer's protocol. Sample libraries were assembled as previously described (Tsai et al., 2014) and sequenced using the Illumina MiSeq platform. Data were analysed using open-source guideseq software (version 1.1) (Tsai et al., 2016). Consolidated reads were mapped to the mouse mm39 reference genome. Upon identification of the genomic regions integrating the dsODNs in the aligned data, off-target sites with maximum six mismatches to the on-target site, which were absent in the background controls, were retained. A summary of the GUIDE-seq results can be found in Supplementary File 1.

AAV production

Pseudo-typed vectors (AAV2 serotype PHP.eB) were produced by the Viral Vector Facility of the Neuroscience Center Zurich. Briefly, AAV vectors were ultracentrifuged and diafiltered. Physical titers (vector genomes per milliliter, vg/mL) were determined using a Qubit 3.0 fluorometer (Thermo Fisher Scientific) as previously published (Düring et al., 2020). The identity of the packaged genomes of each AAV vector was confirmed by Sanger sequencing.

Animal studies

Animal experiments were performed in accordance with protocols approved by the Kantonales Veterinäramt Zürich and in compliance with all relevant ethical regulations. C57BL/6J mice were housed in a pathogen-free animal facility at the Institute of Pharmacology and Toxicology of the University of Zurich. Mice were kept in a temperature– and humidity-controlled room on a 12-hour light-dark cycle. Mice were fed a standard laboratory chow (Kliba Nafag no. 3437 with 18.5% crude protein) with ad libitum access to food and water. Exclusion criteria were pre-defined during study design to meet ethical regulations. No animal was excluded from the study.

Stereotactic injections in mice

Unless stated otherwise, adult female C57BL/6J mice at P50-P60 were used to introduce a unilateral lesion in the medial forebrain bundle. Buprenorphine [0.1 mg/kg bodyweight], was administered to mice subcutaneously 30 min prior to surgery. Animals were anesthetized using isoflurane (5% isoflurane with 1000 mL/min in 100% O_2) and placed into a stereotaxic mouse frame on a warming surface to maintain body temperature. Anesthesia was maintained at 1.5-2.5% isoflurane with 400 mL/min in 100% O_2 during surgeries. Mice were pre-treated with desipramine [25 mg/kg bodyweight] and pargyline [5 mg/kg bodyweight] 30 min before the injection of 6-hydroxydopamine (6-OHDA) was performed. 6-OHDA was dissolved in 0.02% ascorbate/saline solution at a concentration of 15 mg/mL and used within a maximum of 3h. 3.6µg of 6-OHDA were injected into the medial forebrain bundle (mfb) at the following coordinates (relative to bregma): –1.2 mm anteroposterior (AP); 1.3 mm mediolateral (ML); –5 mm dorsoventral (DV). Sham-injected mice were injected with 0.02% ascorbate/saline solution. Injections were performed using a 5µL Hamilton syringe with a 33G needle at a speed of 0.05 µL/min. The needle was slowly removed 3min after the injection and the wound was sutured using Vicryl 5-0 suture (Ethicon). Animals with unilateral lesions received extensive post-operative care for two weeks. After the lesion, animals received daily glucose injections, and kitten milk (Royal Canin) for one week to support recovery.

4-5 weeks after the introduction of the 6-OHDA lesion, AAVs were injected into the substantia nigra, striatum, or visual cortex at the following coordinates (relative to bregma): –3.0 mm anteroposterior (A/P), 1.2 mm mediolateral (M/L), –4.5 mm dorsoventral (D/V) for the substantia nigra pars compacta; 0.38 mm A/P, 1.8 mm M/L, –4:0.4:-2.4 mm D/V for the striatum; and –4.5 mm A/P, 2.7 mm ML, 0.35 mm D/V for the visual cortex. Injections were performed using the same size needle, syringe, and speed as before. The needle was slowly removed 3min after the injection and the wound was sutured using Vicryl 5-0 suture (Ethicon).

Behavioral assays

Behavior experiments were performed at 4 weeks after the 6-OHDA lesion and 12 weeks after delivery of the treatment. Scientists performing and analyzing behavioral data were blinded during the study. To analyze spontaneous rotations during the dark phase of the light cycle, mice were individually placed into a glass cylinder (10cm diameter, 14cm height) and after 1min of habituation mouse behavior was recorded from the bottom using a digital camera. For assessment of spontaneous rotations after treatment, animals were first habituated to the experimental environment on three separate days. Full body ipsi– and contralateral turns (360°) were counted for 10min. A frame-by-frame video player (VLC media player) was used for scoring. Data are expressed as a percentage of ipsilateral rotations from total rotations.

To assess forelimb akinesia during the light phase of the light cycle, we quantified left and right forelimb usage in the stepping test (Blume et al., 2009; Olsson et al., 1995). First, the animal was allowed to settle at one edge of the table (~2s) with all limbs on the table. Next, the experimenter lifted the hind legs of the mouse by pulling up the tail, leaving only the forepaws touching the table. Animals were pulled backwards by the tail at a steady pace of approximately 1m in 3-4s for a total distance of 1m. Two trials of three consecutive repetitions were performed per animal with at least 10min break between the two trials. Behavior was recorded from the side using a digital camera and the number of adjusting steps from both forepaws was counted. Data are represented as percentage of ipsilateral steps from total steps.

For assessing drug-induced rotations, D-amphetamine (5 mg/kg bodyweight; Sigma-Aldrich) or apomorphine (0.5 mg/kg bodyweight; Sigma-Aldrich) was administered to mice via intraperitoneal injections. Following the injection, mice were placed in a recovery cage for 10min. Afterwards, mice were placed in a cylinder (10cm diameter, 15cm height) and habituated for 1min. Rotations induced by D-amphetamine or apomorphine were recorded from the bottom for 10min using a digital camera and only fully-body turns (360°) were counted as previously described. Data are expressed as percentage of ipsilateral or contralateral rotations from total rotations.

Trans-cardiac perfusion, brain isolation, and dissection of brain regions

Sodium pentobarbital (Kantonsapotheke Zürich) was injected via intraperitoneal injection at a dose of 100mg/kg. Complete anesthesia was confirmed by the absence of a toe pinch reflex. Mice were placed on a perfusion stage inside a collection pan and the peritoneal cavity was exposed. The diaphragm was cut through laterally and the rib cage was cut parallel to the lungs, creating a chest “flap”. The flap was clamped in place using a hemostat (Fine Science Tools) and a 25G needle (Sterican), attached to silicon tubing and a peristaltic pump, was inserted into the left ventricle. The right atrium was cut for drainage. Animals were first perfused with ice-cold PBS (Thermo Fisher Scientific) at a rate of 10mL/min, followed by perfusion with ice-cold fixative at the same rate (4% paraformaldehyde, PFA, Sigma-Aldrich). Once the perfusion was complete, mice were decapitated and the skull was removed with scissors and tweezers without inflicting damage to the underlying tissue. The brain was removed using a spatula.

For histology, PFA-perfused brains were post-fixated in 4% PFA for 4h, followed by overnight incubation in 30% sucrose. For neurotransmitter quantifications, brains were isolated, rinsed in PBS, and cut into 1mm slices using an acrylic mouse brain matrix (AgnThos) and razor blades. The striatum was isolated under a stereomicroscope using the mouse brain atlas (Paxinos and Franklin, 2001). For amplicon sequencing, regions of interest (striatum or SNc) were manually dissected from 40µm-thick coronal sections under a stereomicroscope using the mouse brain atlas (Paxinos and Franklin, 2001).

Immunohistochemistry

Fresh or snap-frozen PFA-fixed brain tissues of C57BL/6J mice were cut into 40µm-thick sections using a microtome. Sections were blocked in PBS supplemented with 5% normal donkey serum (cat. no. ab7475, abcam) and 0.3% Triton X-100 (Sigma-Aldrich) for 1h. Brain sections were incubated with primary antibodies overnight at 4°C (rabbit-NEUN, 1:1'000, abcam 177487; mouse-TH; 1:1'000, Immunostar 22941; chicken-GFAP, 1:1'500, abcam ab95231; rat-BrdU, 1:400, Oxford Biotech OBT0030). Donkey anti-rabbit-488 (1:1'000), donkey anti-mouse-594 (1:500), donkey anti-chicken-647 (1:500) and donkey anti-rat-647 (1:500; all from Jackson ImmunoResearch) were used as secondary antibodies and sections were counterstained with 4',6-diamidino-2-phenylindole (DAPI, Sigma-Aldrich). Mounting was performed using Prolong Gold Antifade Mountant (Thermo Fisher Scientific). Images were taken with a Zeiss LSM 900 or a Zeiss AxioScan.Z1 slidescanner and analyzed with Fiji (Schindelin et al., 2012) or cell profiler (Stirling et al., 2021). The numerical density of cells was estimated using optical dissection (NvVref method). Density of striatal fibres in the lesioned hemisphere was quantified as relative fluorescence intensity (FI) compared to the intact hemisphere. Additionally, the FI of the TH staining detected in the corpus callosum of each hemisphere was used for background correction of the FI detected in the striatum of the same hemisphere. Antibodies are listed in supplementary table 4.

Iterative immunofluorescence imaging (4i) and image analysis

Frozen PFA-fixed brain tissues of C57BL/6J mice were cut into 40µm-thick sections using a microtome. Before mounting the sections, glass-bottomed 24-well plates (Cellvis P24-1.5H-N) were coated with poly-D-lysine (0.1mg/mL, Sigma-Aldrich) for 5min at RT on a shaker. Afterwards, wells were rinsed three times with deionized water and left to dry overnight. Tissue sections were washed three times in PBS and transferred into the coated wells containing 500µL of PBS, which was carefully aspirated with a glass pipette to allow the sections to adhere flat to the bottom. Sections were left to dry until there was no visible liquid remaining around the edges of the sections. Next, tissue sections were rinsed with PBS (3×5min), followed by 1h incubation in blocking solution (PBS supplemented with 3% donkey serum, 0.5% Triton X-100, and 0.025% PFA) at RT. Sections were then incubated in primary antibodies (list in supplementary table 4), diluted in blocking solution, for 3 nights at 4°C. Next, sections were washed in PBS (3×5min), rinsed in blocking solution for 5min, followed by incubation with secondary antibodies and DAPI (1:1000; stock 1mg/mL) for 2h at RT. All following steps were performed under low light conditions to reduce possible fluorophore crosslinking. Last, sections were washed in PBS (3×5min) and imaging buffer (PBS supplemented with N-Acetyl-cysteine at 0.7M final concentration, pH 7.4) was added at least 5min prior to imaging to guarantee penetrance of tissue sections. Once the imaging cycle had finished, sections were rinsed three times with dH_20 and incubated in equal amounts of dH_20 and elution buffer (3×5min; 0.5M L-glycine, 3M urea, 3M guanidine hydrochloride, 0.07M TCEP-HCl; pH 2.5). Successful elution of each antibody was visually confirmed using a fluoresence microscope. After elution, tissue sections were washed three times in PBS (5min) and then another 4i round was started. A total of 4 imaging cycles were performed.

All 4i z-stacks (image intervals of 0.5µm) were collected on an ImageXpress Confocal HT confocal laser-scanning microscope with a 20x water objective (NA 0.95) using bi-directional scanning. Samples of the same imaging cycle were labeled with the same antibodies and images were collected with identical microscopy settings for laser power, gain, digital offset, pinhole diameter, and z-step. Images from tile scans were exported using MetaXpress and analyzed using Fiji (Schindelin et al., 2012). DAPI intensity patterns were used to align image tiles from different staining cycles.

In vivo BrdU proliferation assay

Five days after delivery of the treatment, bromodeoxyuridine was administered to mice at a concentration of 0.8 mg/mL via drinking water. Frozen PFA-fixed brain tissues of BrdU-treated mice were cut into 40µm-thick sections using a microtome. Sections were washed 2ξ15min and 1ξ5min in PBS, followed by a 10min incubation in 1M HCl on ice, and a 25min incubation in 2M HCl at 37°C. Next, tissues were rinsed in 0.1M borate buffer (Sigma-Aldrich) for 10min on a shaker at RT. After the tissues were rinsed in PBS for 6ξ10min, brain tissues were stained as described in section “Immunohistochemistry”.

Neurotransmitter purification and UHPLC-ECD quantifications

Snap-frozen fresh striata of lesioned or unlesioned hemispheres were used for the purification of neurotransmitters. All materials were kept cold on dry ice during the whole purification procedure and samples were kept under low light conditions on ice. Tissue samples were powderized with 2 pulses (at maximum intensity) using a CryoPrepTM system (Covaris). Equal amounts of powder were transferred to a pre-cooled 2 mL tube. For homogenization of the tissue powder, a metal ball (Qiagen) and 1mL homogenization buffer (100mM Tris-HCl, 2mM EDTA, pH 7.6 supplemented with protease inhibitor tablet) were added to each tube and samples were homogenized for 2ξ90s at 20 Hz using a TissueLyser II (Qiagen). Next, samples were centrifuged for 20min at maximum speed and 4°C. Lysates were next transferred to fresh pre-cooled tubes and 1M HCl was added to a final concentration of 10% (v/v). Subsequently, lysates were filtered using an Amicon Ultra 0.5 (Sigma-Aldrich) and a table top centrifuge (30min at 4°C and maximum speed). 20µL of the filtered sample was used for quantification of total protein amounts. Protein concentrations were determined using the ABBOT Alinity C System (Abbot, Abbotpark, Illinois, USA, kit-no. 7P5920). 20µL of the filtered sample was used in parallel for quantification of neurotransmitter levels by UHPLC-ECD. Brain monoamine neurotransmitter metabolites were analyzed in the filtered lysate using a modified Thermo Fisher UltiMate 3000 High Sensitivity HPLC Electrochemical System (Thermo Fisher Scientific, Waltham, Massachusetts, USA). Injection volume of each sample was 20 µL and separation of the compounds was achieved using an YMC-Hydrosphere UHPLC column (C18 12 nm, S-2.0 µm, 150 x 30 mm, YMC Inc., Wilmington, NC, USA). As a mobile phase, a 56.7mM sodium phosphate buffer, containing 5mM octanesulphonic acid, 50µM EDTA, 0.28% phosphoric acid (85%), and 23% methanol (pH 2.9-3.1, adjust with concentrated 10M NaOH), was used with an isocratic flow rate of 410 µL/min. The column was maintained at 27°C by a surrounding TCC-3000SD column-thermostat. The analytical cell (Coulometric Cell Model 6011RS, Thermo Fisher Scientific) within the electrochemical detector ECD-3000RS (Thermo Fisher Scientific) was adjusted to a 10mV potential and 100µA gain range for the upstream electrode, plus 400mV potential, plus 500nA gain range for the downstream electrode with a response time of 1s. Data was analyzed using the Chromeleon Chromatography Data System (CDS) Software 7.1.9 (Thermo Fisher) and corrected for the protein concentrations of the respective homogenates. All measurements were performed at the clinical chemistry unit of the Kinderspital Zürich.

Statistical analysis

All statistical analyses were performed using GraphPad Prism 10.2.0 for macOS. If not stated otherwise, data are represented as biological replicates and are depicted as means±standard deviation (s.d.). The sample size was approximated based on so-called Fermi methods and experience from previous base editing studies during experimental design. Sample sizes and the statistical analyses performed are described in the respective figure legends. Data were tested for normality using the Shapiro-Wilk test if not stated otherwise. For all analyses, a *P*-value of $P<0.05$ was considered statistically significant.

Data availability

All data associated with this study are present in the paper. Illumina sequencing data is available under accession number GSE237570 at the Gene Expression Omnibus (GEO) and bioproject number PRJNA1155634 at the NCBI Sequence Read Archive.

Acknowledgements

We thank the Functional Genomics Center Zurich (FGCZ) for technical support and access to instruments at the University of Zurich. We thank Cornelia Schwerdel for technical support during *in vitro* and staining experiments. Annina Denoth Lipuner and Sebastian Jessberger are acknowledged for help with planning and setting up 4i experiments and sharing antibodies. Members of the Schwank, Patriarchi, and Häberle labs are acknowledged for discussions and comments on the manuscript.

Additional information

Funding information

This work was supported by the Swiss National Science Foundation (SNSF) grant no. 310030_185293 (to G.S.) and 310030_196455 (to T.P.), Novartis Foundation for Medical-Biological Research no. FN20-0000000203 (to D.B.), SNSF Spark fellowship no. 196287 (to D.B.), the URPP Itinerare (to G.S. and to D.B.), the Helmut Horten Foundation (to G.S.), and the European Research Council (ERC) under the European Union's Horizon 2020 research and innovation program (grant agreement: 891959; to T.P.).

Author contributions

Conceptualization: D.B. and M.W.; Methodology: D.B. and M.W.; Investigation and Validation: D.B., M.W., J.M., D.F.C., P.I.K., S.A.; Visualization: D.B. and P.I.K.; Formal analysis: D.B., M.W., J.M., D.F.C., P.I.K., S.A., A.C., A.R., J.H., T.P., and G.S.; Resources and Data curation: T.P. and G.S.; Writing – original draft: D.B.; Writing – review&editing: D.B., M.W., J.M., D.F.C, P.I.K., S.A., A.C., A.R., J.H., T.P., and G.S.; Supervision and project administration: D.B. and M.W.; Funding acquisition: D.B., T.P., and G.S..

Competing interest declaration

G.S. is an advisor to Prime Medicine.

Figures and figure supplements

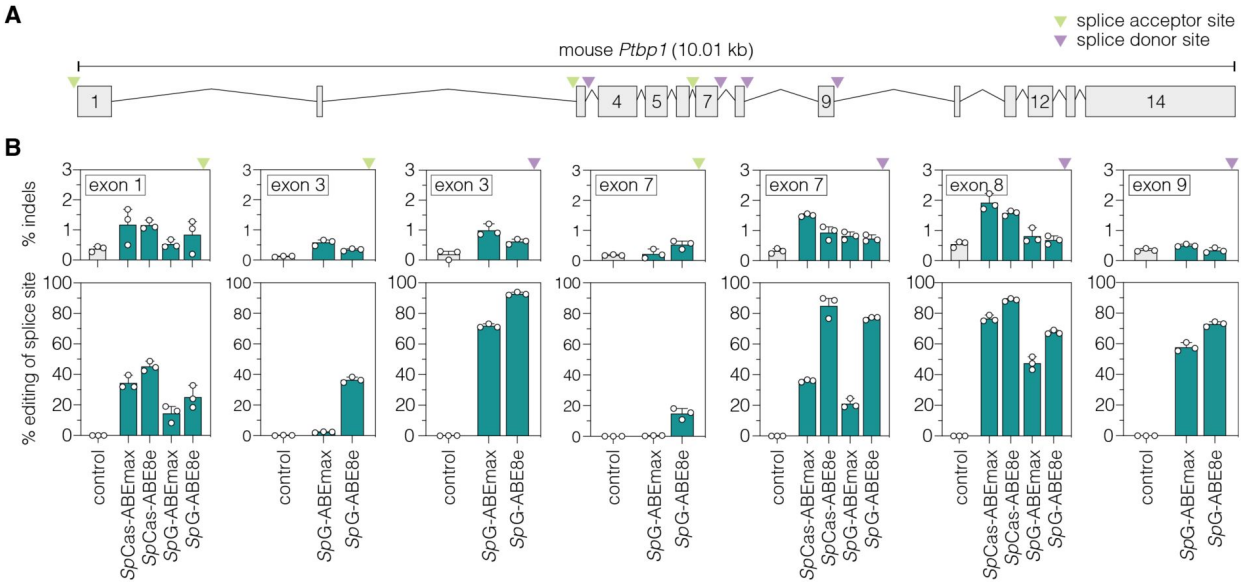

Figure 1 – figure supplement 1

| Adenine base editing of *Ptbp1* splice sites in murine Hepa cells.

(A) Schematic overview of exons and introns of the targeted murine *Ptbp1* locus. sgRNAs target either the conserved GT motif of canonical splice donor sites at the beginning of an intron (purple arrowhead) or the conserved AG motif of canonical splice acceptor sites at the end of an intron (green arrowhead). **(B)** Editing of adenines and indel rates at *Ptbp1* splice donor (purple arrowhead) or acceptor sites (green arrowhead) for *Sp*Cas-or *Sp*G-ABE variants (teal). The targeted exons are indicated in the respective plot. Control samples were transfected with sgRNA (gray). Data are displayed as means±s.d. of three independent experiments. Each datapoint represents one independent experiment. *Ptbp1*, polypyrimidine tract binding protein 1; kb, kilobases; *Sp*Cas, *Streptococcus pyogenes* Cas9 recognizing NGG PAMs; *Sp*G, *Sp*Cas variant recognizing NGN PAMs.

Figure 1 – figure supplement 2

| *In vitro* validation of PTBP1 repression by adenine base editing with sgRNA-ex3 or sgRNA-ex7 in Hepa cells.

(**A**) Editing rates at *Ptbp1* splice donor sites of exon 3 and exon 7. Editing efficiencies were determined by Sanger sequencing and EditR (Kluesner et al., 2018). Control samples were transfected with sgRNA (gray). **(B)** Transcript levels of *Ptbp1* and *Ptbp1*-repressed exons upon adenine base editing in Hepa cells. Transcripts were normalized to *Gapdh*. **(C)** PTBP1 levels in control (1 independent experiment) and edited Hepa cells (2 independent experiments). ACTB protein levels are shown as a loading control. Corresponding sequencing chromatograms for sgRNA-ex3 and sgRNA-ex7 are shown above each sample. Corresponding editing rates are shown below the plots in (B) and (C). Normal distribution of the data was analyzed using the Shapiro-Wilk test. Data are represented as means±s.d. of at least three independent experiments (A,B) and were analyzed using an unpaired two-tailed Student's t-test with Welch's correction (B). Each datapoint represents one independent experiment. Exact *P*-values are indicated in the respective plots. *Ptbp1*, Polypyrimidine tract binding protein 1; *Ptbp2*, Polypyrimidine tract binding protein 2; *Ptbp3*, Polypyrimidine tract binding protein 3; *Kcnq2*, potassium voltage-gates channel subfamily Q member 2; ctrl, control; MW, molecular weight marker.

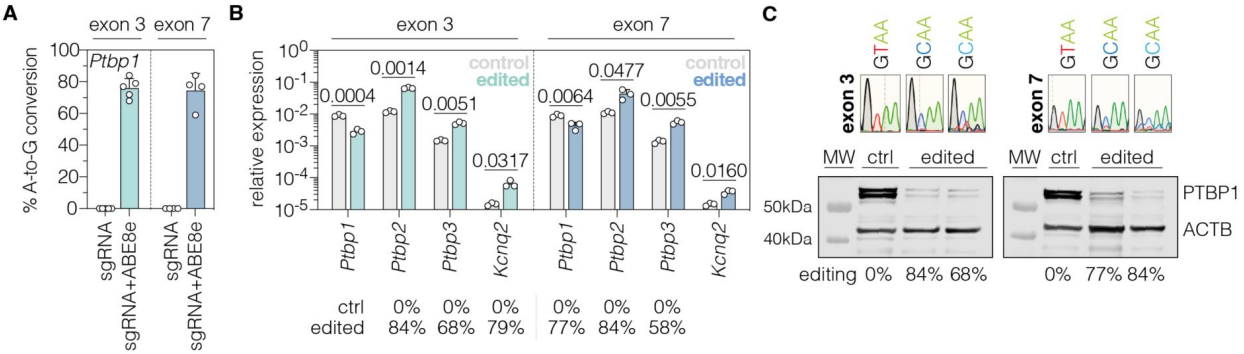

Figure 1 – figure supplement 3

| Adenine base editing generates alternative *Ptbp1* splice sites in cell lines.

(A) Schematic representation of the splice donor at the exon-intron junction of *Ptbp1* exon 3. **(B)** Editing of the canonical splice donor at exon 3 generates alternative *Ptbp1* splice sites in Hepa, N2a, and C8-D1A cells. The correctly spliced isoform is labelled. The corresponding editing rates are shown below each plot. Data of three independent experiments are shown (B). Size of molecular weight (MW) markers in basepairs (bp) are indicated in (B).

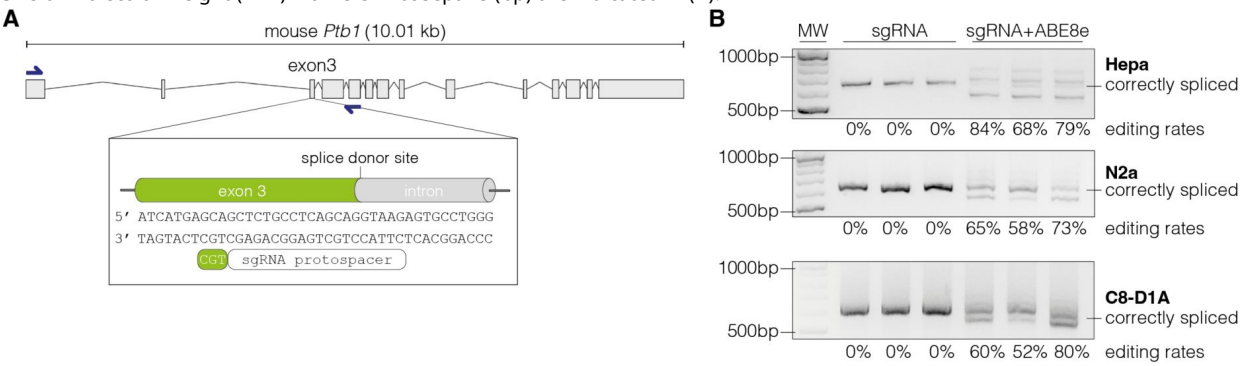

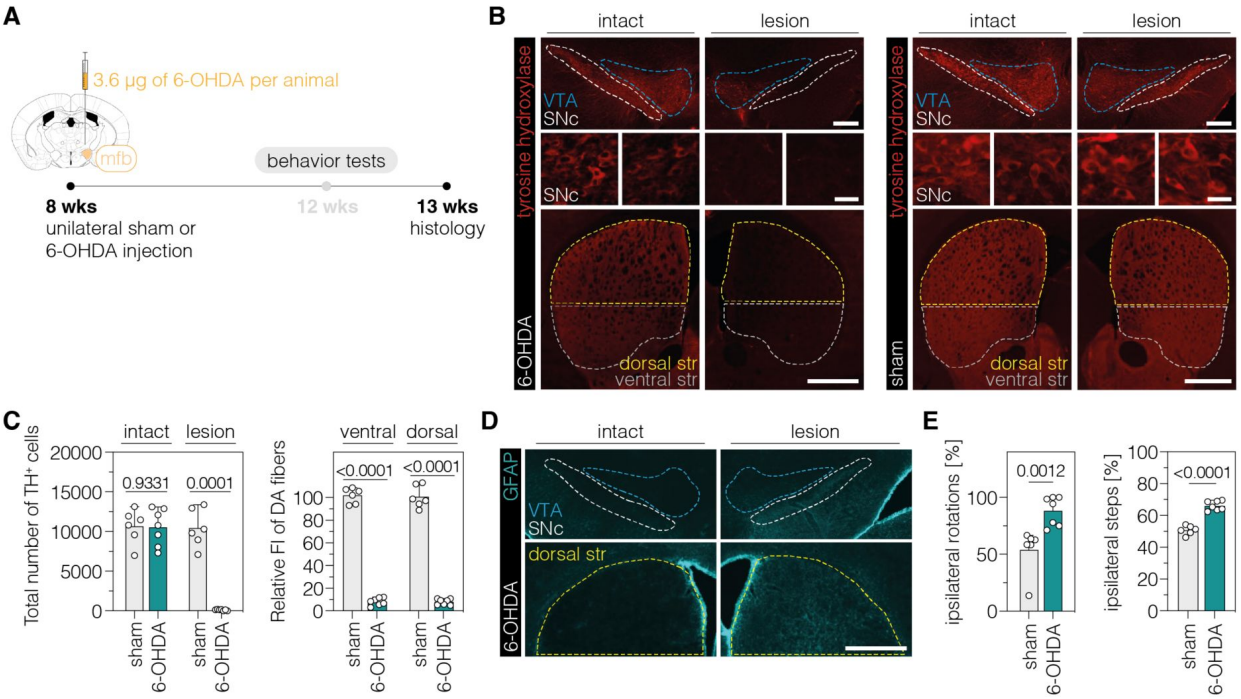

Figure 2 – figure supplement 1

| Validation of the unilateral 6-OHDA lesion in C57BL/6J mice.

(A) Schematic representation of the experimental timeline and setup. **(B)** Representative fluorescence images showing the unilateral loss of TH^+ cells in the SNc (top and middle) and unilateral depletion of DA fibers in the striatum (bottom) in 6-OHDA-lesioned mice (left). Sham-injected animals (right) are shown for comparison. The FI of the TH staining detected in the corpus callosum of each hemisphere was used for background correction of FI detected in the striatum of the same hemisphere. Treatment groups are indicated on the left. **(C)** Quantifications of TH^+ DANs in the SNc (left) and DA fibers in the ventral and dorsal striatum (right). Tissue areas used for quantifications are marked by colored dashed lines in (B). **(D)** Unilateral activation of astrocytes in the SNc (top) and dorsal striatum (bottom) in 6-OHDA-lesioned mice. **(E)** Spontaneous behaviors in sham– and 6-OHDA-lesioned mice. Normal distribution of the data was analyzed using the Shapiro-Wilk test. Data are displayed as means±s.d. of 6-7 mice per group and were analyzed using an unpaired two-tailed Student's t-test with Welch's correction (C, ipsilateral steps in E) or a two-tailed Mann Whitney test (ipsilateral rotations in E). Each datapoint represents one animal. Exact *P*-values are indicated in the respective plots. Scale bars, 20 µm (B, bottom) and 1000 µm (B, top; D). FI, fluorescence intensity; SNc, substantia nigra pars compacta; str, striatum; VTA, ventral tegmental area; GFAP, glial fibrillary acidic protein; TH, tyrosine hydroxylase; DA, dopaminergic.

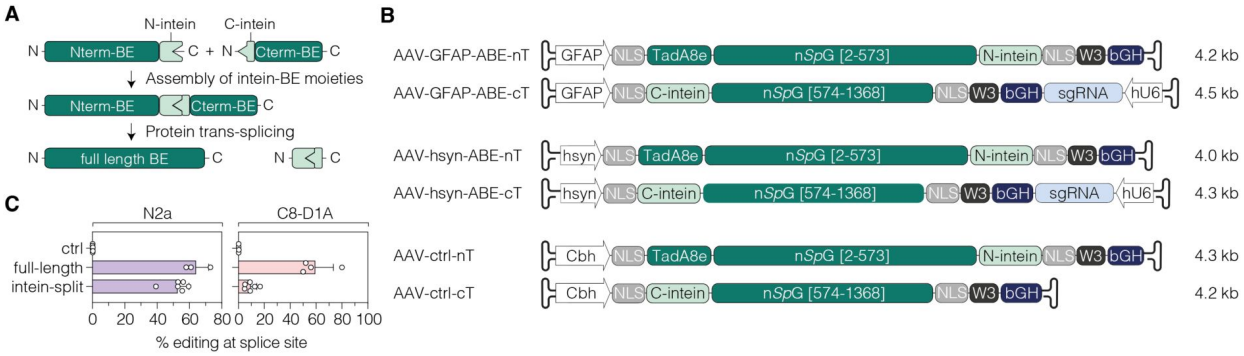

Figure 2 – figure supplement 2

| AAV vector designs for neuronal or astroglial expression of intein-split ABE8e.

(A) Depiction of *Npu* intein-split BE moieties (Nterm-BE and Cterm-BE), forming the full length BE after protein trans-splicing. **(B)** Schematic representation of AAV vector designs with the short GFAP (Lee et al., 2008), hsyn (Kügler et al., 2003), or Cbh promoter (Gray et al., 2011) and their corresponding lengths in kilobase pairs (including ITRs). Constructs are not depicted to scale. **(C)** Editing efficiencies of full-length (CMV promoter) or intein-split ABE expression vectors in N2a (hsyn promoter) and C8-D1A cells (GFAP promoter). Control samples were treated with the sgRNA only. Data of 3-6 independent experiments are displayed as means±s.d. (C). BE, base editor; ABE, adenine base editor; nT/Nterm, N-terminal AAV construct; cT/Cterm, C-terminal AAV construct; GFAP, glial fibrillary acidic protein promoter; hsyn, human synapsin 1 promoter; Cbh, truncated chimeric CMV/chicken b-actin hybrid promoter; NLS, nuclear localization signal; TadA8e, adenosine deaminase; n*Sp*G, *Sp*G nickase; W3, woodchuck hepatitis virus post-transcriptional regulatory element; bGH, bovine growth hormone poly adenylation signal; hU6, human U6 promoter; kb, kilobase pairs.

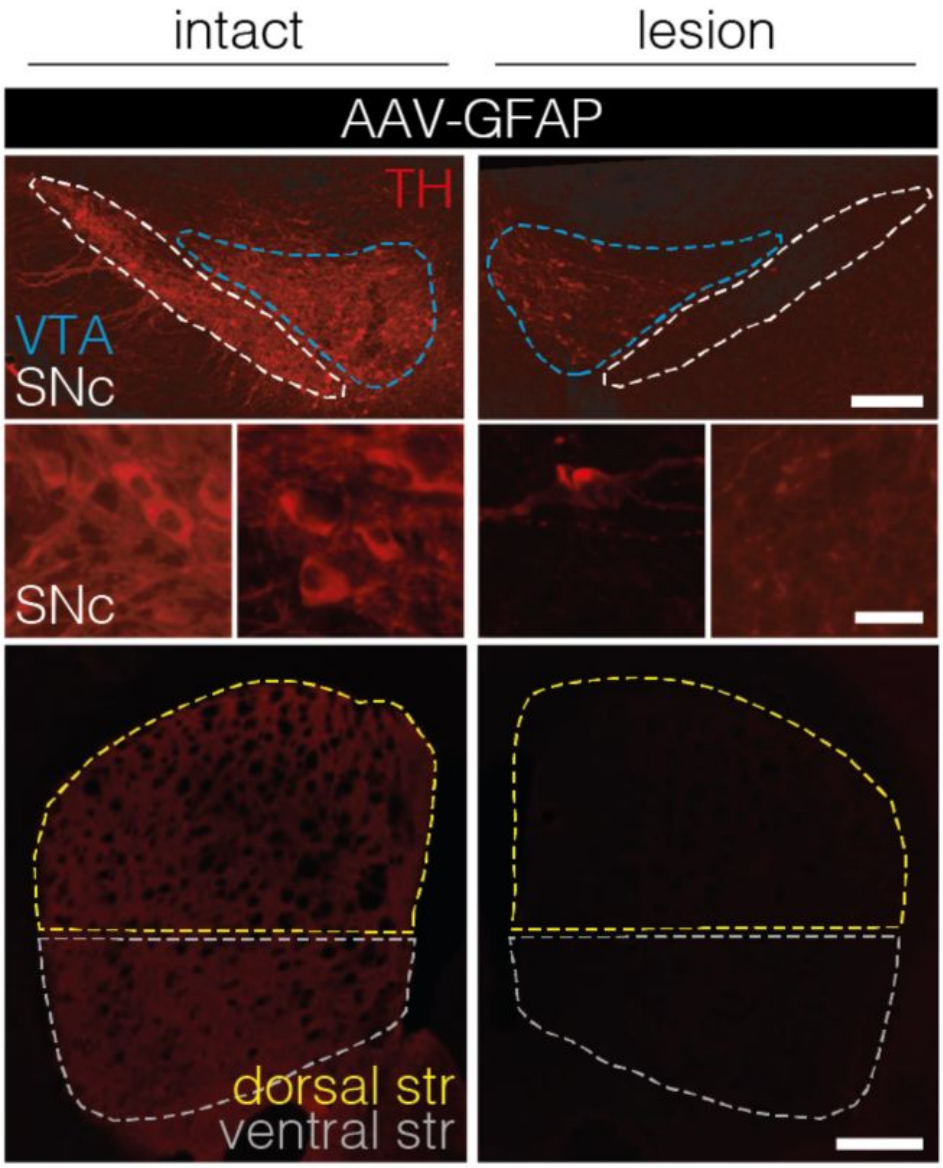

Figure 2 – figure supplement 3

| PTBP1 downregulation in astrocytes of the SNc fails to generate TH$^+$ cells.

Representative images of brain sections showing the intact (left) or lesioned (right) SNc (top and middle) or striatum (bottom) in animals after astroglial PTBP1 downregulation (n=4 mice). The FI of the TH staining detected in the corpus callosum of each hemisphere was used for background correction of FI detected in the striatum of the same hemisphere. Tissue areas used for quantifications are marked by colored dashed lines. Scale bars, 20 µm (middle) and 1000 µm (top and bottom). AAV-GFAP, AAV-GFAP-ABE treatment; GFAP, glial fibrillary acidic protein; SNc, substantia nigra pars compacta; VTA, ventral tegmental area; TH, tyrosine hydroxylase.

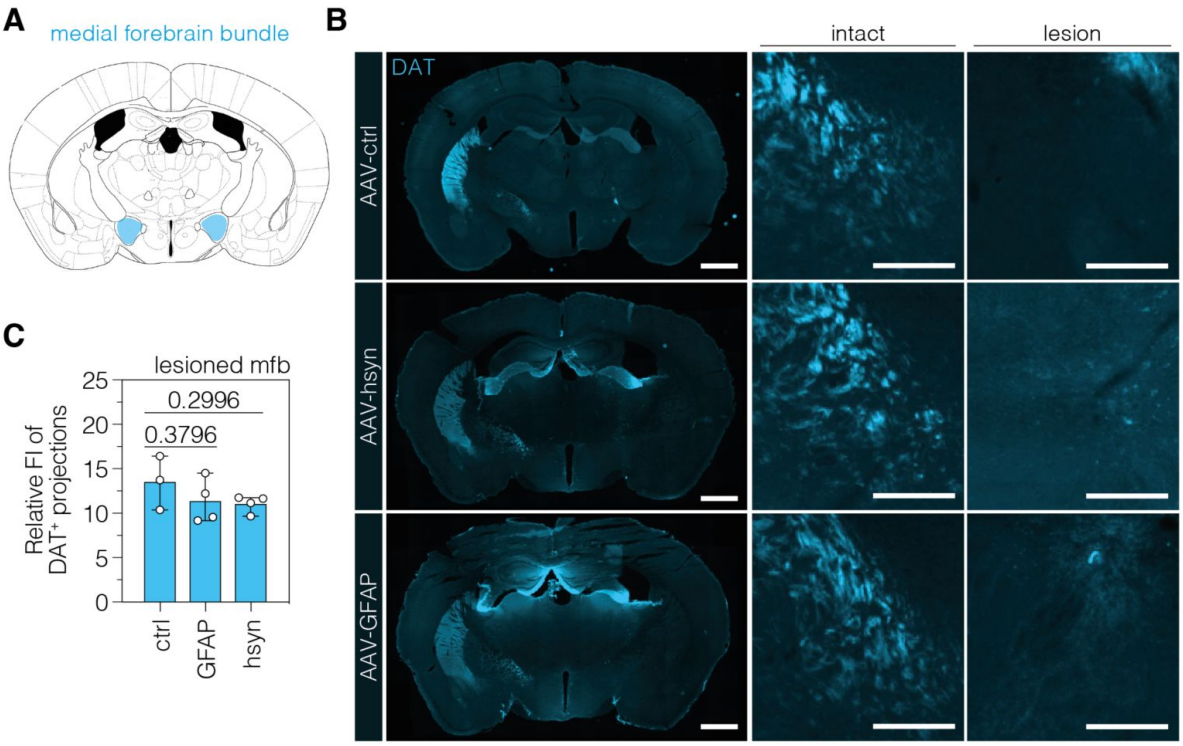

Figure 2 – figure supplement 4

| TH-expressing cells in the SNc do not form neuronal projections through the mfb.

(**A,B**) Schematic depiction of the mfb (A) on the mouse brain atlas (Paxinos and Franklin, 2001) and representative images of DA projections in the mfb of the intact and lesioned hemisphere in treated PD mice. Treatment groups (left) and hemispheres (top) are indicated. **(C)** Quantifications of DA projections in the mfb, assessed as relative fluorescence intensity (FI) of the dopaminergic marker DAT (dopamine transporter) compared to the intact mfb of the same section, in animals treated with AAV-ctrl, AAV-GFAP, or AAV-hsyn. The FI of the DAT staining detected in the thalamus of each hemisphere was used for background correction of FI detected in the mfb of the same hemisphere. Control animals were treated with AAV-PHP.eB particles, expressing the ABE8e variant under the ubiquitous Cbh promoter. Normal distribution of the data was analyzed using the Shapiro-Wilk test. Data are represented as means±s.d. of 3-4 animals per group and were analyzed using a one-way ANOVA with Dunnett's multiple comparisons test. Each datapoint represents one animal. Exact *P*-values are indicated in the respective plots. Scale bars, 1000 µm (left) and 50 µm (middle and right). ctrl, AAV-ctrl-ABE treatment; GFAP, AAV-GFAP-ABE treatment; hsyn, AAV-hsyn-ABE treatment; mfb, medial forebrain bundle; FI, fluorescence intensity; DA, dopaminergic; DAT, dopamine transporter.

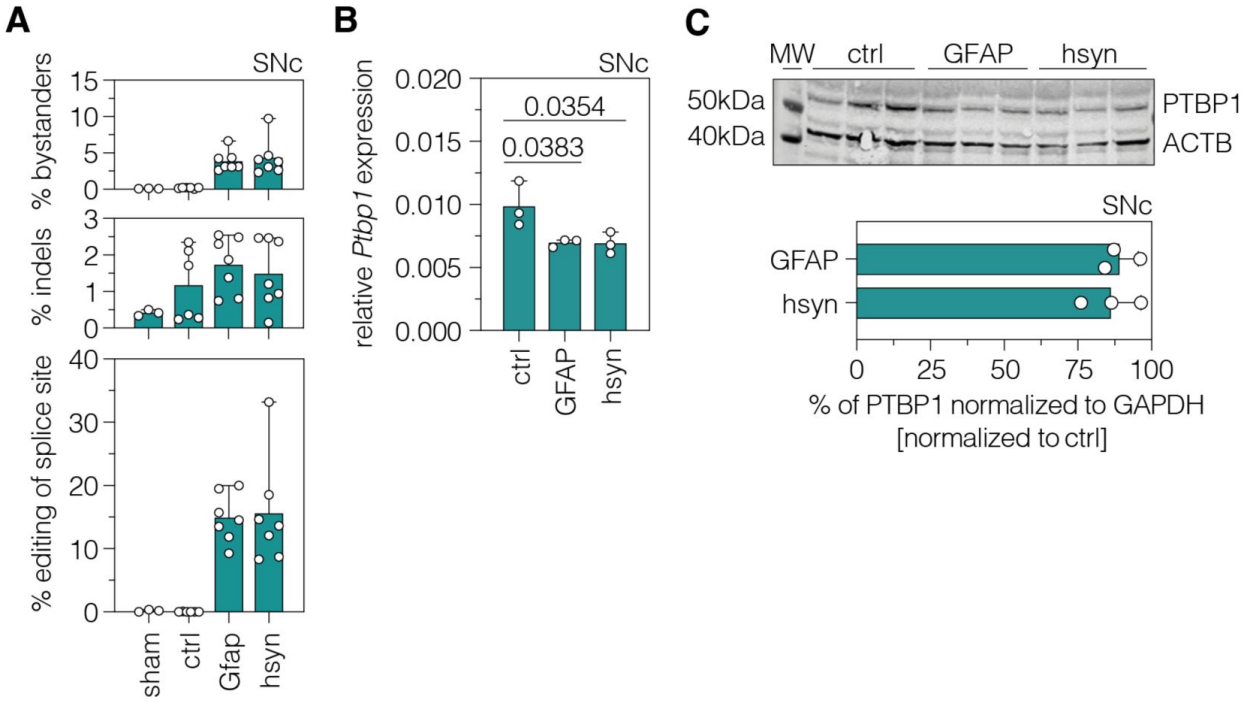

Figure 2 – figure supplement 5

| *In vivo* validation of PTBP1 downregulation by adenine base editing in astrocytes and neurons of the SNc.

(**A**) Quantifications of *in vivo* base editing of adenines and indel rates within the editing window at the targeted *Ptbp1* splice donor. **(B)** Transcript levels of *Ptbp1* upon adenine base editing in the lesioned SNc of AAV-ctrl-, AAV-GFAP-, and AAV-hsyn-treated PD mice. Transcripts were normalized to *Gapdh*. **(C)** PTBP1 levels in the lesioned SNc of treated 6-OHDA-lesioned PD mice (n=3 mice per group). ACTB protein levels are shown as a loading control. PTBP1 abundance was compared to ACTB and normalized to the PTBP1/ACTB ratio of AAV-ctrl-treated animals. Control animals were treated with AAV-PHP.eB particles, expressing the ABE8e variant under the ubiquitous Cbh promoter. Normal distribution of the data was analyzed using the Shapiro-Wilk test. Data are represented as means±s.d. of 3-7 animals per group and were analyzed using a one-way ANOVA with Dunnett's multiple comparisons test (C). Each datapoint represents one animal. Exact *P*-values are indicated in the respective plots. ctrl, AAV-ctrl-ABE treatment; GFAP, AAV-GFAP-ABE treatment; hsyn, AAV-hsyn-ABE treatment; SNc, substantia nigra pars compacta; *Ptbp1*/PTBP1, Polypyrimidine tract binding protein 1; ACTB, beta actin; MW, molecular weight marker.

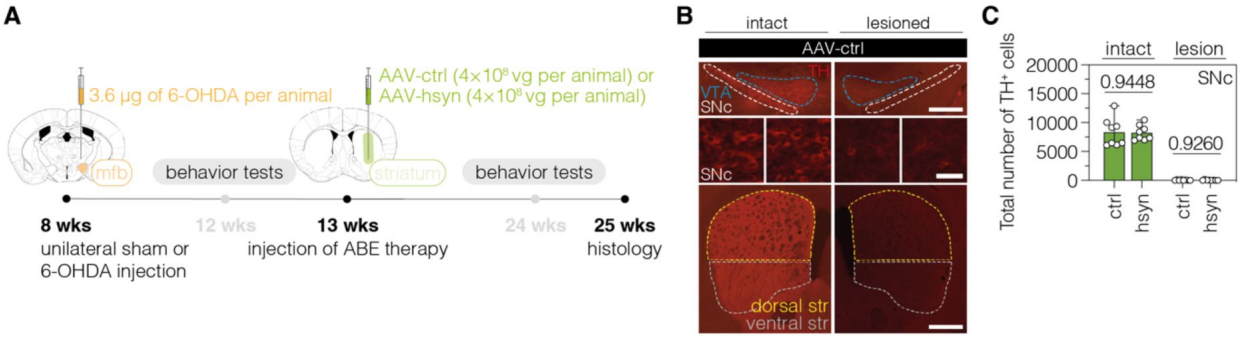

Figure 3 – figure supplement 1

| Validation of the unilateral lesion in 6-OHDA mice after neuronal PTBP1 downregulation in the striatum.

(A) Schematic representation of the experimental timeline and setup. **(B)** Representative fluorescence images showing the unilateral loss of TH^+ cells in the SNc (top and middle) and unilateral depletion of DA fibers in the striatum (bottom) in 6-OHDA-lesioned mice treated with AAV-ctrl. Scale bars, 1000 µm (top and bottom) and 20 µm (middle). **(C)** Quantifications of TH^+ cells in the intact (dark green) and lesioned (light green) SNc after administration of the AAV-hsyn treatment to the striatum. Control animals were treated with AAV-PHP.eB particles, expressing the ABE8e-*Sp*G variant under the Cbh promoter. Tissue areas used for quantifications are marked by colored dashed lines in (B). Normal distribution of the data was analyzed using the Shapiro-Wilk test. Data are displayed as means±s.d. of 8 mice per group and were analyzed using an unpaired two-tailed Student's t-test with Welch's correction (C, "intact") or a two-tailed Mann-Whitney test (C, "lesion"). Each datapoint represents one animal. Exact *P*-values are indicated in the respective plots. ABE, adenine base editor; ctrl, AAV-ctrl-ABE treatment; hsyn, AAV-hsyn-ABE treatment; SNc, substantia nigra pars compacta; VTA, ventral tegmental area; TH, tyrosine hydroxylase.

Figure 3 – figure supplement 2

| *In vivo* validation of PTBP1 downregulation by adenine base editing in neurons of the striatum.

(A) Quantifications of *in vivo* base editing of adenines and indel rates within the editing window at the targeted *Ptbp1* splice donor (n=6-11 mice per group). **(B)** Representative CRISPResso output file showing the frequency and positioning of edited adenines in the lesioned striatum. **(C)** Transcript levels of *Ptbp1* upon adenine base editing in the lesioned striatum. Transcripts were normalized to *Gapdh* (n=3 mice per group). **(D)** PTBP1 levels in the lesioned striatum of treated 6-OHDA-lesioned PD mice (n=3 mice per group). ACTB protein levels are shown as a loading control. PTBP1 abundance was compared to ACTB and normalized to the PTBP1/ACTB ratio of AAV-ctrl-treated animals. Control animals were treated with AAV-PHP.eB particles, expressing the ABE8e variant under the ubiquitous Cbh promoter. Normal distribution of the data was analyzed using the Shapiro-Wilk test. Data are represented as means±s.d. of 3-11 animals per group and were analyzed using an unpaired two-tailed Student's t-test with Welch's correction (B). Each datapoint represents one animal. Exact *P*-values are indicated in the respective plots. ctrl, AAV-ctrl-ABE treatment; hsyn, AAV-hsyn-ABE treatment; str, striatum; *Ptbp1*/PTBP1, Polypyrimidine tract binding protein 1; ACTB, beta actin; MW, molecular weight marker.

Figure 3 – figure supplement 3

| Identification of sgRNA-dependent off-target sites using GUIDE-seq.

(A) Frequency of indels of sgRNA-ex3 and the *Sp*G nuclease (left) and dsODN integrations within the edited reads (right) in N2a cells. **(B)** Experimentally identified off-target sites for the sgRNA-ex3 protospacer targeting the *Ptbp1* locus. The number of reads for the on-target (top) and off-target sites (middle and bottom) as well as the number of mismatches, chromosomal location, and gene annotation are indicated on the right. **(C,D)** Deep sequencing results of the off-target sites (C) and transcript levels (D) of *Mypn* and *Ank1* upon adenine base editing in the lesioned striatum. Transcripts were normalized to *Gapdh* (n=3 mice per group). Data are represented as means±s.d. of 3 animals per group and were analyzed using an unpaired two-tailed Student's t-test with Welch's correction (D).

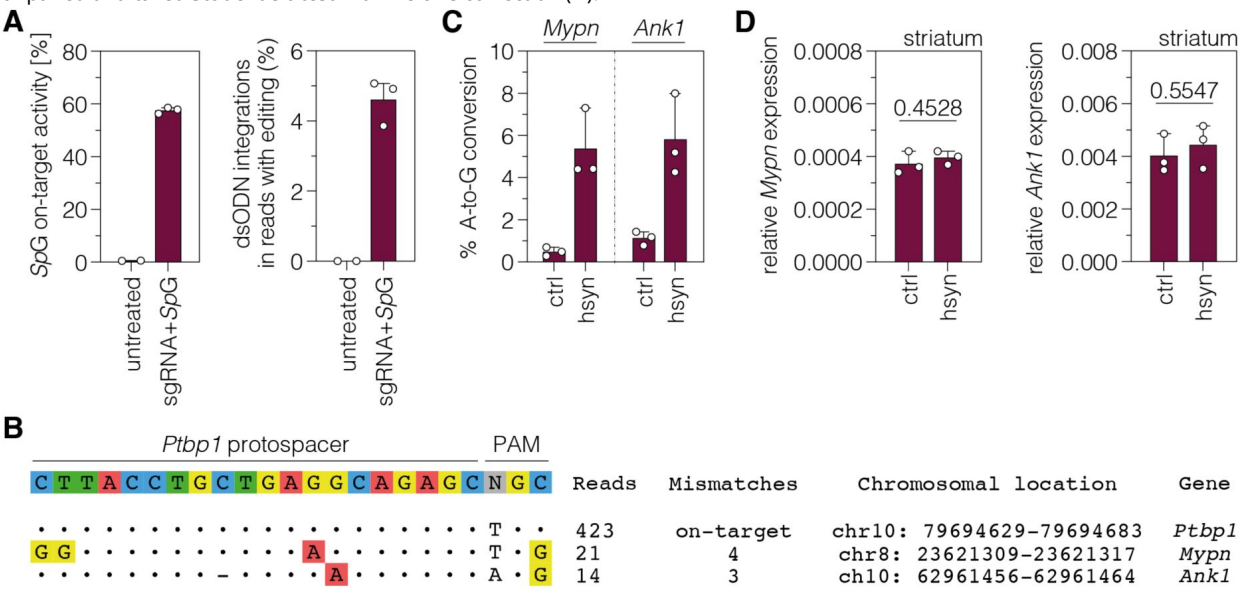

Figure 3 – figure supplement 4

| Neuronal PTBP1 repression in the striatum increases striatal dopamine in 6-OHDA-lesioned hemispheres.

(A) Schematic representation of striatal regions used for neurotransmitter quantifications. (**B,C**) HPLC quantifications of dopamine (B) and its metabolite DOPAC (C) in the intact and lesioned striatum of animals treated with AAV-ctrl or AAV-hsyn. Control animals were treated with AAV-PHP.eB particles, expressing the ABE8e-*Sp*G variant under the Cbh promoter. Neurotransmitter concentrations in nmol were normalized to total protein amounts in g. Normal distribution of the data was analyzed using the Shapiro-Wilk test. Data are displayed as means±s.d. of 5 mice per group and were analyzed using an unpaired two-tailed Student's t-test ("intact" in B; C) or a two-tailed Mann-Whitney test ("lesion" in B). Each datapoint represents one animal. Exact *P*-values are indicated in the respective plots. ctrl, AAV-ctrl-ABE treatment; hsyn, AAV-hsyn-ABE treatment; DOPAC, 3,4-dihydroxyphenylacetic acid; nmol, nanomol; g, gram.

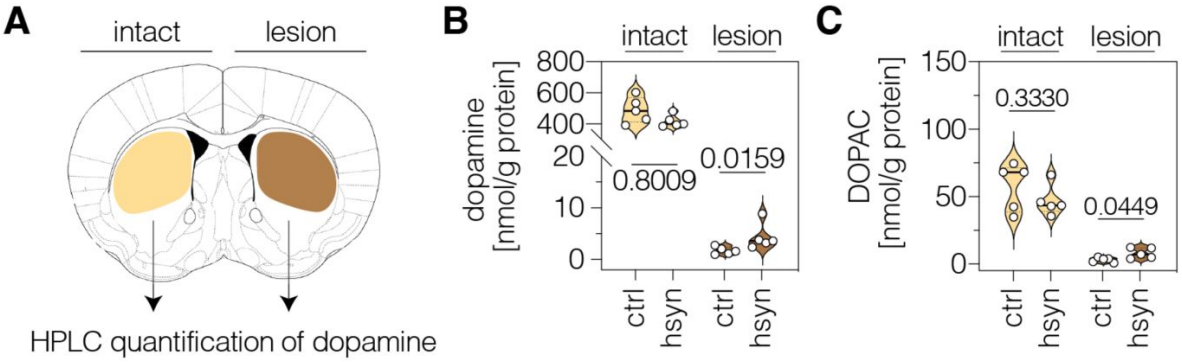

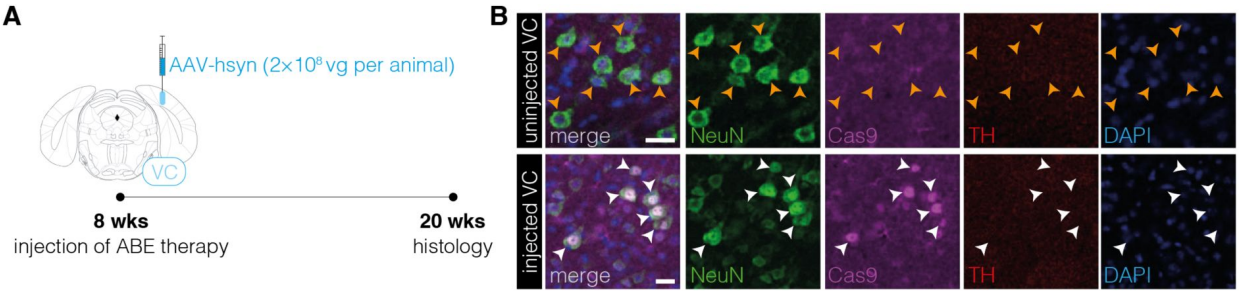

Figure 3 – figure supplement 5

| Absence of TH$^+$ cell bodies in the visual cortex after neuronal PTBP1 downregulation.

(A) Schematic representation of the experimental timeline and setup. **(B)** Representative images showing ABE8e expression in neurons (white arrowheads) of the visual cortex (VC) in the injected hemisphere and absence of TH$^+$ cell bodies after 12 weeks (bottom). Absence of ABE8e expression in neurons (orange arrowheads) of the uninjected hemisphere (top) is shown for comparison (n=3 mice). Scale bars, 20µm. VC, visual cortex; NEUN, hexaribonucleotide binding protein-3; Cas9, *Streptococcus pyogenes* Cas9; TH, tyrosine hydroxylase; DAPI, 4',6-diamidino-2-phenylindole.

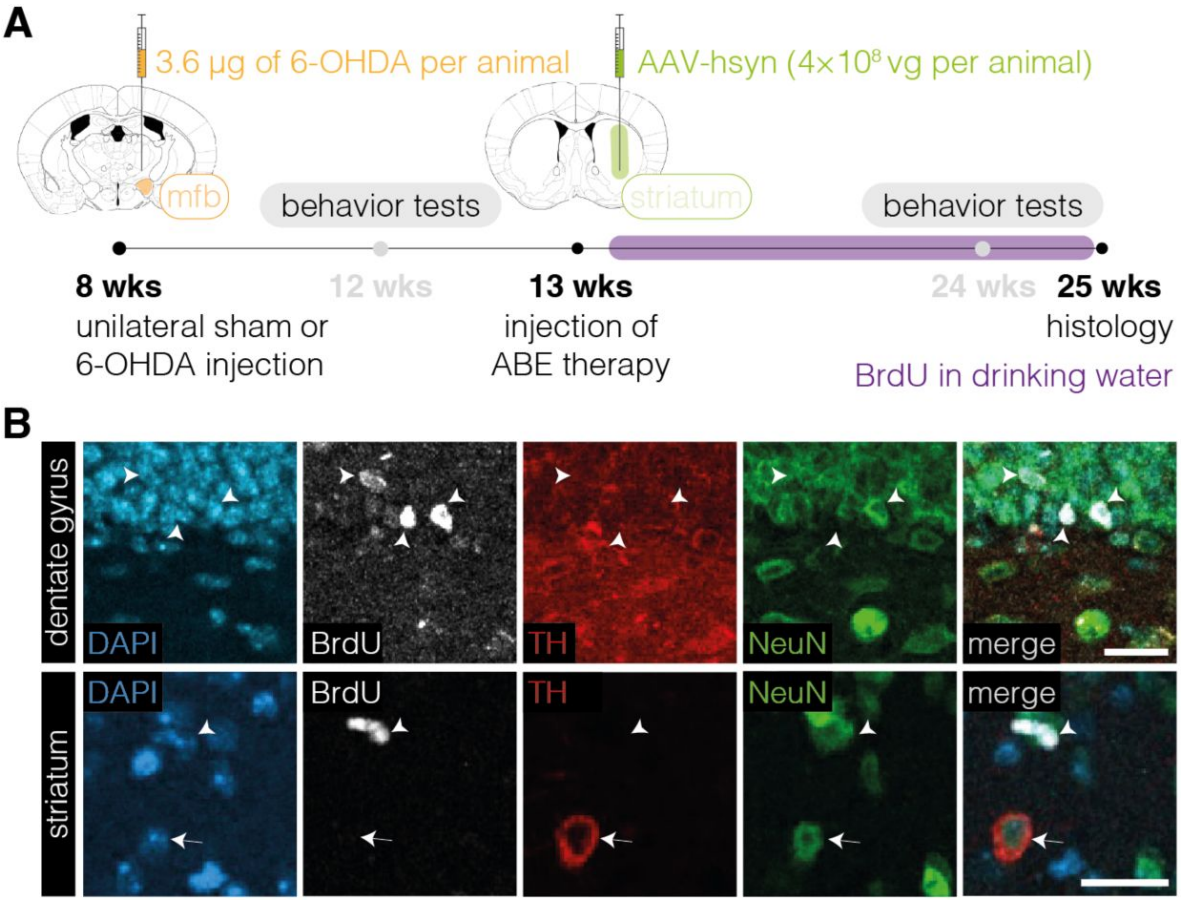

Figure 3 – figure supplement 6

| Absence of proliferation in TH$^+$ cell bodies in the striatum after neuronal PTBP1 downregulation.

(A) Schematic representation of the experimental timeline and setup. (**B**) Representative images of BrdU-labeled cells (white arrowhead) in the dentate gyrus (DG, top) or striatum (bottom) and of TH$^+$ cell bodies (white arrow) in the striatum of animals treated with AAV-hsyn (n=4 mice; n=163 TH$^+$ cell bodies in the striatum). Images of the DG are shown as a positive control (top). Scale bars, 20µm. ABE, adenine base editor; DAPI, 4',6-diamidino-2-phenylindole; BrdU, bromodeoxyuridine; TH, tyrosine hydroxylase; NEUN, hexaribonucleotide binding protein-3.

Figure 4 – figure supplement 1

| Validation of antibodies for 4i experiments.

Antibody specificity was assessed on mouse brain sections of the striatum or SNc (n=2 animals). Representative images of one animal are shown. Scale bars, 50µm. DAPI, 4',6-diamidino-2-phenylindole; SOX2, sex determining region Y-box 2; NES, neuroepithelial stem cell protein; DCX, doublecortin; NEUN, hexaribonucleotide binding protein-3; TH, tyrosine hydroxylase; DAT, dopamine transporter; CTIP2, COUP-TF-interacting protein 2; PV, parvalbumin; CALB2, calbindin 2; SST, somatostatin.

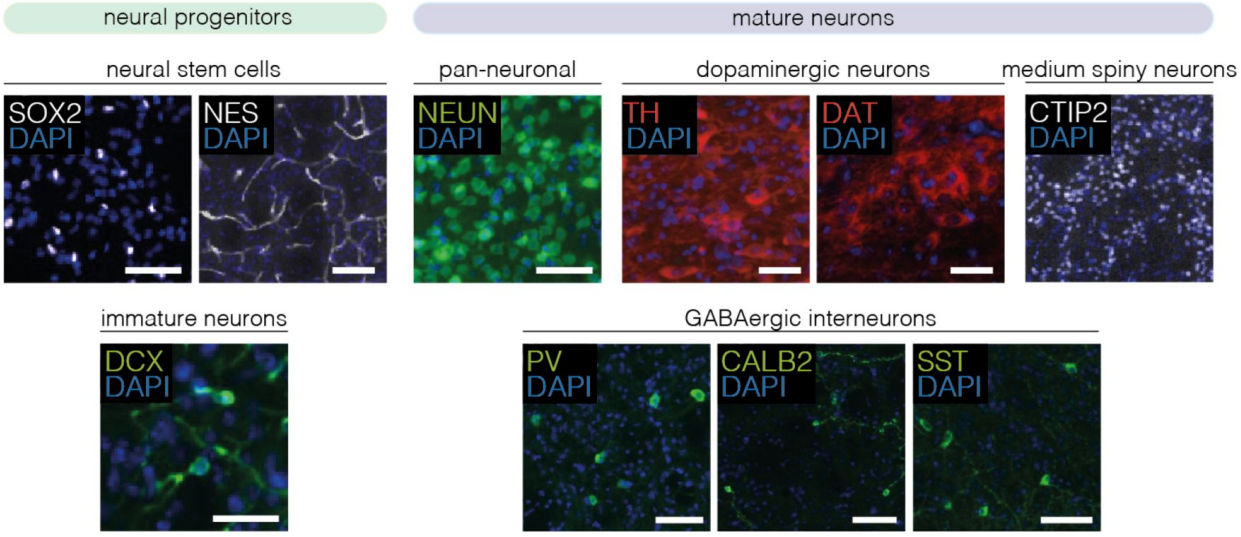

Figure 5 – figure supplement 1

| Neuronal PTBP1 downregulation in the SNc alleviates drug-free motor dysfunction in 6-OHDA-lesioned PD mice.

(**A,B**) Spontaneous behaviors, assessed as contralateral forelimb akinesia in the stepping test (A) and spontaneous rotations in the cylinder test (B), in animals treated in the SNc. (**C,D**) Drug-induced rotations, assessed as amphetamine-induced ipsilateral rotations (C) and apomorphine-induced contralateral rotations (D), in animals treated in the SNc. Normal distribution of the data was analyzed using the Shapiro-Wilk test. Data are represented as means±s.d. of 3-4 animals per group and were analyzed using a two-way ANOVA with Šidák's multiple comparisons test. Each datapoint represents one animal. Exact *P*-values are indicated in each plot. hsyn, AAV-hsyn-ABE treatment; GFAP, AAV-GFAP-ABE treatment; ctrl, AAV-ctrl-ABE treatment.

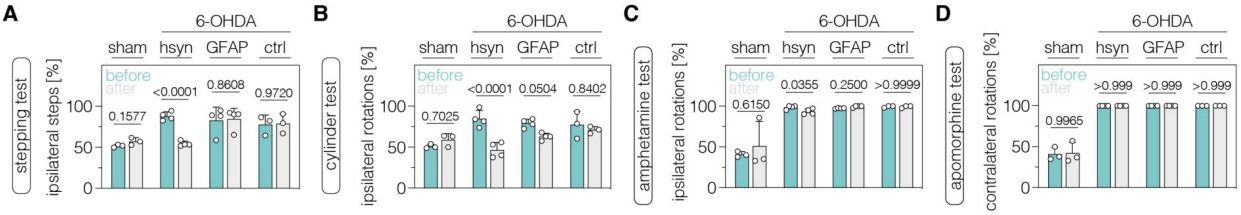

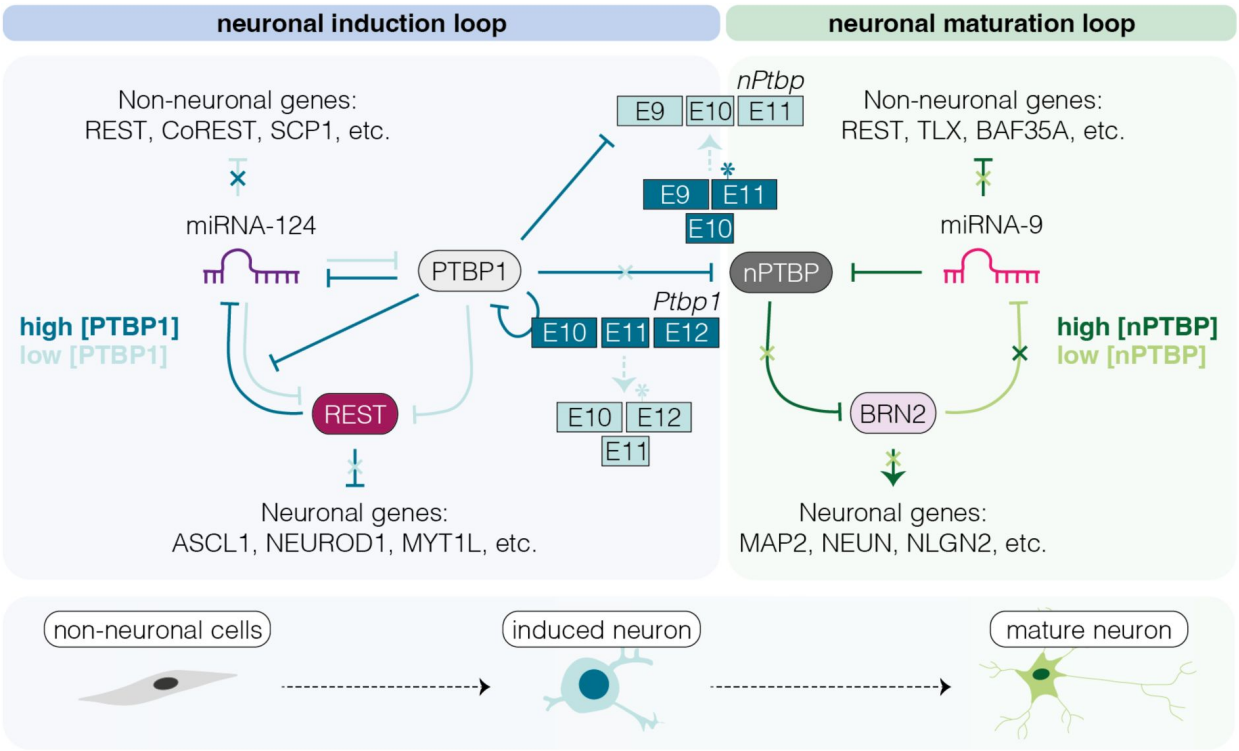

Figure 5 – figure supplement 2

| Schematic representation of the PTBP1/nPTBP regulatory loops driving neuronal differentiation and maturation.

The dynamic regulation of PTBP1-mediated inhibition of miRNA-124, which acts on components of the REST complex to activate neuronal-specific expression programs in non-neuronal cells is a key event in the miRNA-124/REST signaling cascade. High PTBP1 expression in non-neuronal cells blocks miRNA-124-induced neuronal differentiation. During neuronal differentiation (low [PTBP1]), miRNA-124 represses PTBP1, enabling expression of nPTBP, pro-neuronal transcription factors, and consequently neuron-specific splicing events that eventually lead to neuronal maturation (Makeyev et al., 2007; Xue et al., 2013).

Supplementary table 1

Oligos used for cloning of sgRNA plasmids.

oligo name	sgRNA_ID	sequence (5′ → 3′)
sgRNA01_PTBP1_fwd	sgRNA-01	CACCGACTTACCCGTCCATGGCACA
sgRNA01_PTBP1_rev		AAACTGTGCCATGGACGGGTAAGTC
sgRNA02_PTBP1_fwd	sgRNA-02	CACCGCTTACCTGCTGAGGCAGAGC
sgRNA02_PTBP1_rev		AAACGCTCTGCCTCAGCAGGTAAGC
sgRNA03_PTBP1_fwd	sgRNA-03	CACCGTTCTCAGCGGGGATCCGACG
sgRNA03_PTBP1_rev		AAACCGTCGGATCCCCGCTGAGAAC
sgRNA04_PTBP1_fwd	sgRNA-04	CACCGACTCACCAGCTTGGCATGCT
sgRNA04_PTBP1_rev		AAACAGCATGCCAAGCTGGTGAGTC
sgRNA05_PTBP1_fwd	sgRNA-05	CACCGCCCACAGTCCCTGGATGGCC
sgRNA05_PTBP1_rev		AAACGGCCATCCAGGGACTGTGGGC
sgRNA06_PTBP1_fwd	sgRNA-06	CACCGCTTACCAAAGGCTGCTGCCA
sgRNA06_PTBP1_rev		AAACTGGCAGCAGCCTTTGGTAAGC
sgRNA07_PTBP1_fwd	sgRNA-07	CACCGAATACCTGCGGCCTGAGGGA
sgRNA07_PTBP1_rev		AAACTCCCTCAGGCCGCAGGTATTC
sgRNA08_PTBP1_fwd	sgRNA-08	CACCGACATACCTCAGGGTTCAGAT
sgRNA08_PTBP1_rev		AAACATCTGAACCCTGAGGTATGTC

Supplementary table 2

Oligos used for cloning of AAV plasmids.

oligo name	sequence (5′ → 3′)
pGfap-AAV-fwd	CGGCCTCTAGATCAGGGTACCAACATATCCTGGTGTGGAGTAGGG
pGfap-AAV-rev	CGGCCTCTAGATCAGGGTACCAACATATCCTGGTGTGGAGTAGGG
phsyn-AAV-fwd	CGGCCTCTAGATCAGGGTACCGAGGGCCCTGCGTATGAG
phsyn-AAV-rev	CTGTCCGTTTCATGGTGGCACCGGTCCAACTCTCGACTGCGCTC

Supplementary table 3

Oligos used for RT-qPCR.

oligo name	sequence (5′ → 3′)
Gapdh-RTqPCR_fwd	CATCACTGCCACCCAGAAGACTG
Gapdh-RTqPCR_rev	ATGCCAGTGAGCTTCCCGTTCAG
Ptbp1-RTqPCR_fwd	CACCGCTTCAAGAAACCAGGCT
Ptbp1-RTqPCR_rev	GTTGCTGGAGAAGAGGCTCTTG
Ptbp2-RTqPCR_fwd	CCTGTAACACTTGATGTCCTTCAC
Ptbp2-RTqPCR_rev	CACCATACTGGAGCAAAGCCTG
Ptbp3-RTqPCR_fwd	CTCGCTGGTTTCCCGGAG
Ptbp3-RTqPCR_rev	TCCCCGCTTTAAACCGACTG
Kcnq2-RTqPCR_fwd	GTCTTCTCCTGCCTTGTGCT
Kcnq2-RTqPCR_rev	GCAGCCCAGATCCTCACAAA

Supplementary table 4

List of antibodies used in this study.

antibody	clone	host species	dilution	application
NEUN	EPR12763	rabbit	1:1’000	histology, primary
GFAP	ab95231	chicken	1:1’500	histology, primary
TH	na	mouse	1:1’000	histology&4i, primary
TH	ab76442	chicken	1:500	histology, primary
*Sp*Cas9	7A9-3A3	mouse	1:50	histology, primary
BrdU	BU1/75 (ICR1)	rat	1:400	histology, primary
DCX	sc-8066	goat	1:300	4i, primary
Nestin	EPR22023	rabbit	1:100	4i, primary
Sox2	14-9811-82	rat	1:300	4i, primary
DAT	ab184451	rabbit	1:300	4i, primary
CTIP2	25B6	rat	1:500	4i, primary
PV	EPR13091	goat	1:100	4i, primary
SST	G10	mouse	1:250	4i, primary
CALB2	6B3	mouse	1:250	4i, primary
anti-rabbit AF488	JIR-711-545-152	donkey	1:1’000	histology, secondary
anti-rabbit Cy3	JIR-711-165-152	donkey	1:500	histology, secondary

antibody	clone	host species	dilution	application
anti-chicken Cy5	JIR-703-175-155	donkey	1:500	histology, secondary
anti-mouse Cy3	JIR-715-165-151	donkey	1:500	histology, secondary
anti-goat AF488	JIR-705-545-003	donkey	1:1’000	histology, secondary
anti-goat Cy5	JIR-705-175-147	donkey	1:5000	histology, secondary
anti-rat Cy5	JIR-712-175-153	donkey	1:500	histology, secondary
PTBP1	EPR9048B	rabbit	1:10’000	Western blot, primary
ACTB	ab8226	mouse	1:2’000	Western blot, primary
IRDye® 680RD anti-rabbit IgG	926-68073	donkey	1:20’000	Western blot, secondary
IRDye® 800CW anti-mouse IgG	926-32212	donkey	1:20’000	Western blot, secondary

oligo name	sequence (5′ → 3′)
PTBP1.ex1-HTS_fwd	CTTTCCCTACACGACGCTCTTCCGATCTNNNNNNTTCTGCTATTCCTGCGCCTC
PTBP1.ex1-HTS_rev	GGAGTTCAGACGTGTGCTCTTCCGATCTNNNNNNCATTGCAGCGGTTAGAGGGA
PTBP1.ex3-HTS_fwd	CTTTCCCTACACGACGCTCTTCCGATCTNNNNNNTGCAAATGGGAATGCAGGAA
PTBP1.ex3-HTS_rev	GGAGTTCAGACGTGTGCTCTTCCGATCTNNNNNNCAGGTCCTTTCTCCCAGCTC
PTBP1.ex7.1-HTS_fwd	CTTTCCCTACACGACGCTCTTCCGATCTNNNNNNATGCCAAGCTGGTGAGTAGG
PTBP1.ex7.1-HTS_rev	GGAGTTCAGACGTGTGCTCTTCCGATCTNNNNNNGCAGGTCAGGTCGAGTGTAG
PTBP1.ex7.2-HTS_fwd	CTTTCCCTACACGACGCTCTTCCGATCTNNNNNNCTACACTCGACCTGACCTGC
PTBP1.ex7.2-HTS_rev	GGAGTTCAGACGTGTGCTCTTCCGATCTNNNNNNATCACTGCACCTCACCTCAC
PTBP1.ex8-HTS_fwd	CTTTCCCTACACGACGCTCTTCCGATCTNNNNNNGTCAGCCTCTCCGTATGCAG
PTBP1.ex8-HTS_rev	GGAGTTCAGACGTGTGCTCTTCCGATCTNNNNNNCCTGTGGATGCTTCTGGAGG
PTBP1.ex9-HTS_fwd	CTTTCCCTACACGACGCTCTTCCGATCTNNNNNNGGTGCTGGGAATTCTGTCCT
PTBP1.ex9-HTS_rev	GGAGTTCAGACGTGTGCTCTTCCGATCTNNNNNNCAGCAGTGGCAGATAGAGGG
Mypn1_HTS_fwd	CTTTCCCTACACGACGCTCTTCCGATCTNNNNNNGGTCAAAAATGGCGCAAGGT
Mypn1_HTS_rev	GGAGTTCAGACGTGTGCTCTTCCGATCTNNNNNNTGCACACACTGACAAGGACT
Ank1_HTS_fwd	CTTTCCCTACACGACGCTCTTCCGATCTNNNNNNTGTTTTCTGCTTCTCAGGGGA
Ank1_HTS_rev	GGAGTTCAGACGTGTGCTCTTCCGATCTNNNNNNCAGTGGTCCAAGACCGTACA

Supplementary table 5

Oligos used for deep sequencing.

Supplementary table 6

Reference nucleotide sequences of amplicons for deep sequencing.

amplicon name	amplicon sequence (5′→ 3′)
PTBP1.ex1	TTCTGCTATTCCTGCGCCTCCGCTCCGTTCCCCGCGGGTCTCTTCCGTGTGCCATGGA CGGGTAAGTCCTGCCGCGCCCCTCGCACGCCGCTCCGCTCACCACTCCGTCCCAGCCA TCGCTGCCGCGCGCGTGGACTTTTGGCCCCCGCCGATCCCTCTAACCGCTGCAATG
PTBP1.ex3	TGCAAATGGGAATGCAGGAAAGGAATCAGCCTGGAACTAAGATTCCATGCTCTCTTCT CAGCGGGGATCCGACGAGCTCTTCTCCACGTGTGTCAGCAACGGCCCCTTCATCATGA GCAGCTCTGCCTCAGCAGGTAAGAGTGCCTGGGTGCCCTAGGGAGTCCTGCCTTGACA GGTACAGGGCGAGCTGGGAGAAAGGACCTG
PTBP1.ex7.1	ATGCCAAGCTGGTGAGTAGGACTTGCTTGGGTGGGCAATCCTATGACTGGCCCACGCA CTCACCTATGGCTCCCCACAGTCCCTGGATGGCCAGAACATCTACAACGCCTGCTGCA CGCTGCGCATCGACTTCTCCAAGCTCACCAGTCTCAATGTCAAGTACAACAATGATAA GAGCAGAGACTACACTCGACCTGACCTGC
PTBP1.ex7.2	CTACACTCGACCTGACCTGCCCTCTGGAGACAGCCAGCCTTCACTAGACCAGACCATG GCAGCAGCCTTTGGTAAGATGCTGTACTGAGACACACCAAATGAACAGGGGTGGGACA GGCCACCTAGCTGTCAGGGCACCCTGGCACTGCACAGCCCAGCCACTCAGCAGTCCTG CCCGTGCCTGGCCCAGCCGTGAGGTGAGGTGCAGTGAT
PTBP1.ex8	GTCAGCCTCTCCGTATGCAGGAGCCGGGTTCCCTCCCACCTTTGCCATCCCTCAGGCC GCAGGTATTCACGCTCATCCTGACCCCAGCGCCTGCATGCCCACACAGCCCCATAACT GTCCATAGACCGGGATGCCACTGGCCCCAAGTGTTAGGCCCCAGGCCCCCTTCCTTCT GGGGAGAGGGGAAGGGGCCTCCAGAAGCATCCACAGG
PTBP1.ex9	GGTGCTGGGAATTCTGTCCTTTTGGTCAGCAATCTGAACCCTGAGGTATGTGGGTATT GCTGTGCTCTGCTTATACATGGAGTAGTGGTGGGGTGCTGACTGACCACAAGTCAGGG TGGGGGAGCATACTGGATGGCAAGCAGGGTTTCTGGGTGTCCCAGGCGCCGTGTGGGT ATAGGCGTGCTGCCCCTCTATCTGCCACTGCTG

amplicon name	amplicon sequence (5′→ 3′)
Mypn-OT1	GGTCAAAAATGGCGCAAGGTCAGAGGGCACCGTGGGTTCCAGCACACCTGCCCGCAGC GCTTCATCCATAGGCCCTGAGCTACCACCCAGCTCTGCTTCAGCAGGTACCCAGTACA GCTTGAGGTCAGCAGCTTGCTCCCATGCCTGTTCTTTGCTTTGCAAATGAGTCCTTGT CAGTGTGTGCA
Ank1-OT2	TGTTTTCTGCTTCTCAGGGGAGAATCAGCTGTTCTGGCCATTTGATGGTACAGGGTTT GCCCATTCGAAGCCGACTCAGCCCTGCTCTGTCTCACAGGTAAGCACACGAGATCCCC CTTTTCTGGAGCCCTCCAGCGACCCCACTCACCACAGTGAACAGAAGTTGTACGGTCT TGGACCACTG

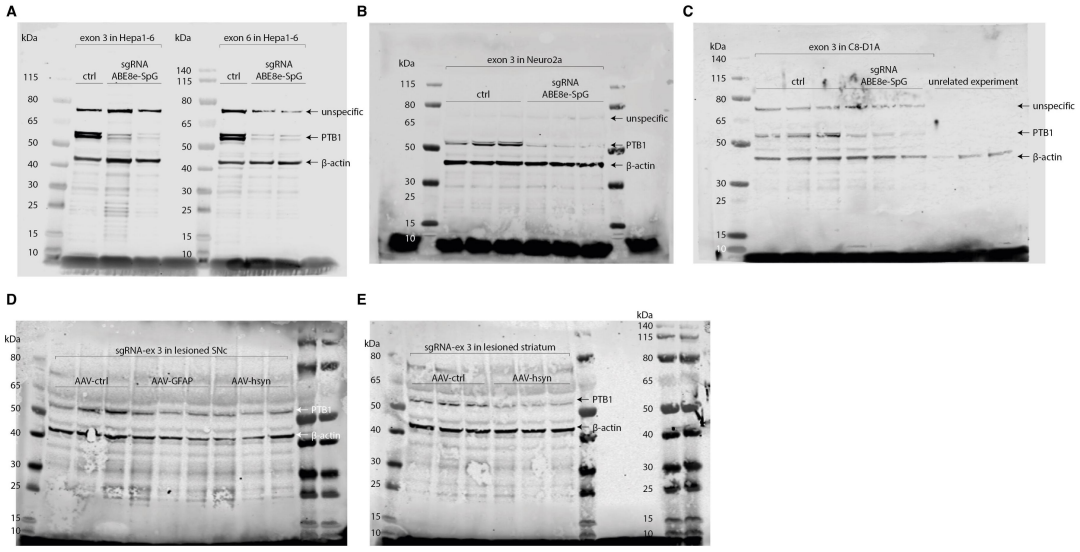
A
kDa
exon 3 in Hepa1-6
ctrl
sgRNA ABE8e-SpG
115
80
65
50
40
30
25
15
10
kDa
exon 6 in Hepa1-6
ctrl
sgRNA ABE8e-SpG
140
115
80
65
50
40
30
25
15
10
unspecific
PTB1
β-actin
B
kDa
exon 3 in Neuro2a
ctrl
sgRNA ABE8e-SpG
115
80
65
50
30
25
15
10
unspecific
PTB1
β-actin
C
kDa
exon 3 in C8-D1A
ctrl
sgRNA ABE8e-SpG
unrelated experiment
140
115
80
65
50
30
25
15
10
unspecific
PTB1
β-actin
D
kDa
sgRNA-ex 3 in lesioned SNc
AAV-ctrl
AAV-GFAP
AAV-hsyn
80
65
50
40
30
25
15
10
PTB1
β-actin
E
kDa
sgRNA-ex 3 in lesioned striatum
AAV-ctrl
AAV-hsyn
140
115
80
65
50
40
30
25
15
10
PTB1
β-actin

References

1. Adikusuma F, Piltz S, Corbett MA, Turvey M, McColl SR, Helbig KJ, Beard MR, Hughes J, Pomerantz RT, Thomas PQ (2018) **Large deletions induced by Cas9 cleavage** *Nature* https://doi.org/10.1038/s41586-018-0380-z

2. Alber S *et al.* (2023) **PTBP1 regulates injury responses and sensory pathways in adult peripheral neurons** *Sci Adv* **9** https://doi.org/10.1126/SCIADV.ADI0286/SUPPL_FILE/SCIADV.ADI0286_DATA_S1_AND_S2.ZIP

3. Arenas E (2020) **Method to combat Parkinson's disease by astrocyte-to-neuron conversion** *Nat 2021 5827813* **582**:489–490 https://doi.org/10.1038/d41586-020-01817-4

4. Arroyo-García LE, Vázquez-Roque RA, Díaz A, Treviño S, De La Cruz F, Flores G, Rodríguez-Moreno A. (2018) **The Effects of Non-selective Dopamine Receptor Activation by Apomorphine in the Mouse Hippocampus** *Mol Neurobiol* **55** https://doi.org/10.1007/s12035-018-0991-2

5. Bamford NS, Wightman RM, Sulzer D (2018) **Dopamine's Effects on Corticostriatal Synapses during Reward-Based Behaviors** *Neuron* **97**:494–510 https://doi.org/10.1016/J.NEURON.2018.01.006

6. Bloem BR, Okun MS, Klein C (2021) **Parkinson's disease** *Lancet* **397**:2284–2303 https://doi.org/10.1016/S0140-6736(21)00218-X

7. Blume SR, Cass DK, Tseng KY (2009) **Stepping test in mice: A reliable approach in determining forelimb akinesia in MPTP-induced Parkinsonism** *Exp Neurol* **219** https://doi.org/10.1016/j.expneurol.2009.05.017

8. Böck D *et al.* (2022) **In vivo prime editing of a metabolic liver disease in mice** *Sci Transl Med* **14** https://doi.org/10.1126/scitranslmed.abl9238

9. Boix J, Padel T, Paul G (2015) **A partial lesion model of Parkinson's disease in mice – Characterization of a 6-OHDA-induced medial forebrain bundle lesion** *Behav Brain Res* **284** https://doi.org/10.1016/j.bbr.2015.01.053

10. Boutz PL, Stoilov P, Li Q, Lin CH, Chawla G, Ostrow K, Shiue L, Ares M, Black DL (2007) **A post-transcriptional regulatory switch in polypyrimidine tract-binding proteins reprograms alternative splicing in developing neurons** *Genes Dev* **21**:1636–1652 https://doi.org/10.1101/GAD.1558107

11. Brown RC, Lockwood AH, Sonawane BR (2005) **Neurodegenerative diseases: An overview of environmental risk factors** *Environ Health Perspect* https://doi.org/10.1289/ehp.7567

12. Buffo A, Rite I, Tripathi P, Lepier A, Colak D, Horn AP, Mori T, Götz M (2008) **Origin and progeny of reactive gliosis: A source of multipotent cells in the injured brain** *Proc Natl Acad Sci U S A* **105** https://doi.org/10.1073/pnas.0709002105

13. Chen W, Zhen Q, Huang Q, Ma S, Li M (2022) **Repressing PTBP1 fails to convert reactive astrocytes to dopaminergic neurons in a 6-hydroxydopamine mouse model of Parkinson's disease** *Elife* **11** https://doi.org/10.7554/ELIFE.75636

14. Clement K *et al.* (2019) **CRISPResso2 provides accurate and rapid genome editing sequence analysis** *Nat Biotechnol* https://doi.org/10.1038/s41587-019-0032-3

15. Cohen DE, Melton D (2011) **Turning straw into gold: Directing cell fate for regenerative medicine** *Nat Rev Genet* https://doi.org/10.1038/nrg2938

16. Cole JD, Del Castillo JS, Gut G, Gonzalez-Bohorquez D, Pelkmans L, Jessberger S (2022) **Characterization of the neurogenic niche in the aging dentate gyrus using iterative immunofluorescence imaging** *Elife* **11** https://doi.org/10.7554/ELIFE.68000

17. Cunha SR, Mohler PJ (2009) **Ankyrin protein networks in membrane formation and stabilization** *J Cell Mol Med* **13** https://doi.org/10.1111/J.1582-4934.2009.00943.X

18. da Conceição FSL, Ngo-Abdalla S, Houzel JC, Rehen SK (2010) **Murine model for Parkinson's disease: From 6-OH dopamine lesion to behavioral test** *J Vis Exp* https://doi.org/10.3791/1376

19. de Lau LM, Breteler MM (2006) **Epidemiology of Parkinson's disease** *Lancet Neurol* https://doi.org/10.1016/S1474-4422(06)70471-9

20. Delignat-Lavaud B *et al.* (2023) **Synaptotagmin-1-dependent phasic axonal dopamine release is dispensable for basic motor behaviors in mice** *Nat Commun 2023 141* **14**:1–24 https://doi.org/10.1038/s41467-023-39805-7

21. Düring DN *et al.* (2020) **Fast Retrograde Access to Projection Neuron Circuits Underlying Vocal Learning in Songbirds** *Cell Rep* **33** https://doi.org/10.1016/j.celrep.2020.108364

22. Duvoisin R, Ayuk MA, Rinaldi G, Suttiprapa S, Mann VH, Lee CM, Harris N, Brindley PJ (2012) **Human U6 promoter drives stronger shRNA activity than its schistosome orthologue in Schistosoma mansoni and human fibrosarcoma cells** *Transgenic Res* **21** https://doi.org/10.1007/s11248-011-9548-0

23. Elbaz A, Dufouil C, Alpérovitch A (2007) **Interaction between genes and environment in neurodegenerative diseases** *Comptes Rendus – Biol* https://doi.org/10.1016/j.crvi.2007.02.018

24. Filomena MC *et al.* (2020) **Myopalladin promotes muscle growth through modulation of the serum response factor pathway** *J Cachexia Sarcopenia Muscle* **11** https://doi.org/10.1002/JCSM.12486

25. Filomena MC *et al.* (2021) **Myopalladin knockout mice develop cardiac dilation and show a maladaptive response to mechanical pressure overload** *Elife* **10** https://doi.org/10.7554/ELIFE.58313

26. Freyberg Z *et al.* (2016) **Mechanisms of amphetamine action illuminated through optical monitoring of dopamine synaptic vesicles in Drosophila brain** *Nat Commun* **7** https://doi.org/10.1038/ncomms10652

27. Gaudelli NM, Komor AC, Rees HA, Packer MS, Badran AH, Bryson DI, Liu DR (2017) **Programmable base editing of T to G C in genomic DNA without DNA cleavage** *Nature* https://doi.org/10.1038/nature24644

28. Gerfen CR, Surmeier DJ (2011) **Modulation of striatal projection systems by dopamine** *Annu Rev Neurosci* **34**:441–466 https://doi.org/10.1146/ANNUREV-NEURO-061010-113641

29. Gitler AD, Dhillon P, Shorter J (2017) **Neurodegenerative disease: Models, mechanisms, and a new hope** *DMM Dis Model Mech* https://doi.org/10.1242/dmm.030205

30. Glajch KE, Fleming SM, Surmeier DJ, Osten P (2012) **Sensorimotor assessment of the unilateral 6-hydroxydopamine mouse model of Parkinson's disease** *Behav Brain Res* **230** https://doi.org/10.1016/j.bbr.2011.12.007

31. Gray SJ, Foti SB, Schwartz JW, Bachaboina L, Taylor-Blake B, Coleman J, Ehlers MD, Zylka MJ, McCown TJ, Samulski RJ (2011) **Optimizing promoters for recombinant adeno-associated virus-mediated gene expression in the peripheral and central nervous system using self-complementary vectors** *Hum Gene Ther* **22** https://doi.org/10.1089/hum.2010.245

32. Grieger JC, Samulski RJ (2005) **Packaging Capacity of Adeno-Associated Virus Serotypes: Impact of Larger Genomes on Infectivity and Postentry Steps** *J Virol* https://doi.org/10.1128/jvi.79.15.9933-9944.2005

33. Guo Z, Zhang L, Wu Z, Chen Y, Wang F, Chen G (2014) **In vivo direct reprogramming of reactive glial cells into functional neurons after brain injury and in an Alzheimer's disease model** *Cell Stem Cell* **14** https://doi.org/10.1016/j.stem.2013.12.001

34. Han A, Stoilov P, Linares AJ, Zhou Y, Fu XD, Black DL (2014) **De Novo Prediction of PTBP1 Binding and Splicing Targets Reveals Unexpected Features of Its RNA Recognition and Function** *PLoS Comput Biol* **10** https://doi.org/10.1371/journal.pcbi.1003442

35. Hoang T, Kim DW, Appel H, Ozawa M, Zheng S, Kim J, Blackshaw S (2023) **Ptbp1 deletion does not induce astrocyte-to-neuron conversion** *Nat 2023 6187964* **618**:E1–E7 https://doi.org/10.1038/s41586-023-06066-9

36. Iancu R, Mohapel P, Brundin P, Paul G (2005) **Behavioral characterization of a unilateral 6-OHDA-lesion model of Parkinson's disease in mice** *Behav Brain Res* **162** https://doi.org/10.1016/j.bbr.2005.02.023

37. Jiang Y, Wang Y, Huang Z (2021) **Targeting PTB as a One-Step Procedure for In Situ Astrocyte-to-Dopamine Neuron Reprogramming in Parkinson's Disease** *Neurosci Bull* **37** https://doi.org/10.1007/S12264-021-00630-X

38. Kalia L V., Lang AE (2015) **Parkinson's disease** *Lancet* https://doi.org/10.1016/S0140-6736(14)61393-3

39. Karam CS, Williams BL, Jones SK, Javitch JA (2022) **The Role of the Dopamine Transporter in the Effects of Amphetamine on Sleep and Sleep Architecture in Drosophila** *Neurochem Res* **47** https://doi.org/10.1007/s11064-021-03275-4

40. Kluesner MG *et al.* (2021) **CRISPR-Cas9 cytidine and adenosine base editing of splice-sites mediates highly-efficient disruption of proteins in primary and immortalized cells** *Nat Commun* **12** https://doi.org/10.1038/s41467-021-22009-2

41. Kluesner MG, Nedveck DA, Lahr WS, Garbe JR, Abrahante JE, Webber BR, Moriarity BS (2018) **EditR: A Method to Quantify Base Editing from Sanger Sequencing** *Cris J* **1**:239–250 https://doi.org/10.1089/CRISPR.2018.0014

42. Koblan LW *et al.* (2021) **In vivo base editing rescues Hutchinson–Gilford progeria syndrome in mice** *Nature*

43. Komor AC, Kim YB, Packer MS, Zuris JA, Liu DR (2016) **Programmable editing of a target base in genomic DNA without double-stranded DNA cleavage** *Nature* https://doi.org/10.1038/nature17946

44. Kosicki M, Tomberg K, Bradley A (2018) **Repair of double-strand breaks induced by CRISPR–Cas9 leads to large deletions and complex rearrangements** *Nat Biotechnol* https://doi.org/10.1038/nbt.4192

45. Kreitzer AC, Malenka RC (2008) **Striatal Plasticity and Basal Ganglia Circuit Function** *Neuron* **60**:543–554 https://doi.org/10.1016/J.NEURON.2008.11.005

46. Kügler S, Kilic E, Bähr M (2003) **Human synapsin 1 gene promoter confers highly neuron-specific long-term transgene expression from an adenoviral vector in the adult rat brain depending on the transduced area** *Gene Ther* https://doi.org/10.1038/sj.gt.3301905

47. Lee Y, Messing A, Su M, Brenner M (2008) **GFAP promoter elements required for region-specific and astrocyte-specific expression** *Glia* **56** https://doi.org/10.1002/glia.20622

48. Levy JM, Yeh WH, Pendse N, Davis JR, Hennessey E, Butcher R, Koblan LW, Comander J, Liu Q, Liu DR (2020) **Cytosine and adenine base editing of the brain, liver, retina, heart and skeletal muscle of mice via adeno-associated viruses** *Nat Biomed Eng* https://doi.org/10.1038/s41551-019-0501-5

49. Li J, Sun W, Wang B, Xiao X, Liu XQ (2008) **Protein trans-splicing as a means for viral vector-mediated in vivo gene therapy** *Hum Gene Ther* https://doi.org/10.1089/hum.2008.009

50. Li Q, Zheng S, Han A, Lin C-H, Stoilov P, Fu X-D, Black DL (2014) **The splicing regulator PTBP2 controls a program of embryonic splicing required for neuronal maturation** *Elife* **3** https://doi.org/10.7554/elife.01201

51. Lindgren HS, Andersson DR, Lagerkvist S, Nissbrandt H, Cenci MA (2010) **L-DOPA-induced dopamine efflux in the striatum and the substantia nigra in a rat model of Parkinson's disease: Temporal and quantitative relationship to the expression of dyskinesia** *J Neurochem* **112**:1465–1476 https://doi.org/10.1111/J.1471-4159.2009.06556.X

52. Makeyev E V., Zhang J, Carrasco MA, Maniatis T (2007) **The MicroRNA miR-124 Promotes Neuronal Differentiation by Triggering Brain-Specific Alternative Pre-mRNA Splicing** *Mol Cell* **27** https://doi.org/10.1016/J.MOLCEL.2007.07.015

53. Moore DJ, West AB, Dawson VL, Dawson TM (2005) **MOLECULAR PATHOPHYSIOLOGY OF PARKINSON'S DISEASE** *Annu Rev Neurosci* https://doi.org/10.1146/annurev.neuro.28.061604.135718

54. Musunuru K *et al.* (2021) **In vivo CRISPR base editing of PCSK9 durably lowers cholesterol in primates** *Nature* **593** https://doi.org/10.1038/s41586-021-03534-y

55. Niu W, Zang T, Smith DK, Vue TY, Zou Y, Bachoo R, Johnson JE, Zhang CL (2015) **SOX2 reprograms resident astrocytes into neural progenitors in the adult brain** *Stem Cell Reports* **4** https://doi.org/10.1016/j.stemcr.2015.03.006

56. Niu W, Zang T, Zou Y, Fang S, Smith DK, Bachoo R, Zhang CL (2013) **In vivo reprogramming of astrocytes to neuroblasts in the adult brain** *Nat Cell Biol* **15** https://doi.org/10.1038/ncb2843

57. Niu Y, Moghimyfiroozabad S, Moghimyfiroozabad A, Tierney TS, Alavian KN (2021) **The factors for the early and late development of midbrain dopaminergic neurons segregate into two distinct evolutionary clusters** *Brain Disord* **1** https://doi.org/10.1016/J.DSCB.2021.100002

58. Olsson M, Nikkhah G, Bentlage C, Björklund A (1995) **Forelimb akinesia in the rat Parkinson model: Differential effects of dopamine agonists and nigral transplants as assessed by a new stepping test** *J Neurosci* **15** https://doi.org/10.1523/jneurosci.15-05-03863.1995

59. Paxinos G, Franklin KBJ (2001) **The Mouse Brain in Stereotaxic Coordinates** Acad Press

60. Qian C, Dong B, Wang XY, Zhou FQ (2021) **In vivo glial trans-differentiation for neuronal replacement and functional recovery in central nervous system** *Febs J* **288**:4773–4785 https://doi.org/10.1111/FEBS.15681

61. Qian H *et al.* (2020) **Reversing a model of Parkinson's disease with in situ converted nigral neurons** *Nature* https://doi.org/10.1038/s41586-020-2388-4

62. Radhiyanti PT, Konno A, Matsuzaki Y, Hirai H (2021) **Comparative study of neuron-specific promoters in mouse brain transduced by intravenously administered AAV-PHP.eB** *Neurosci Lett* **756** https://doi.org/10.1016/J.NEULET.2021.135956

63. Robel S, Berninger B, Götz M (2011) **The stem cell potential of glia: Lessons from reactive gliosis** *Nat Rev Neurosci* https://doi.org/10.1038/nrn2978

64. Rothgangl T *et al.* (2021) **In vivo adenine base editing of PCSK9 in macaques reduces LDL cholesterol levels** *Nat Biotechnol* https://doi.org/10.1038/s41587-021-00933-4

65. Schindelin J *et al.* (2012) **Fiji: An open-source platform for biological-image analysis** *Nat Methods* https://doi.org/10.1038/nmeth.2019

66. Shimada IS, LeComte MD, Granger JC, Quinlan NJ, Spees JL (2012) **Self-renewal and differentiation of reactive astrocyte-derived neural stem/progenitor cells isolated from the cortical peri-infarct area after stroke** *J Neurosci* **32** https://doi.org/10.1523/JNEUROSCI.4303-11.2012

67. Shin HY, Wang C, Lee HK, Yoo KH, Zeng X, Kuhns T, Yang CM, Mohr T, Liu C, Hennighausen L (2017) **CRISPR/Cas9 targeting events cause complex deletions and insertions at 17 sites in the mouse genome** *Nat Commun* https://doi.org/10.1038/ncomms15464

68. Sirko S *et al.* (2013) **Erratum: Reactive glia in the injured brain acquire stem cell properties in response to sonic hedgehog (Cell Stem Cell** *Cell Stem Cell* https://doi.org/10.1016/j.stem.2013.04.007

69. Stirling DR, Swain-Bowden MJ, Lucas AM, Carpenter AE, Cimini BA, Goodman A (2021) **CellProfiler 4: improvements in speed, utility and usability** *BMC Bioinformatics* **22** https://doi.org/10.1186/s12859-021-04344-9

70. Stoker TB, Barker RA (2020) **Recent developments in the treatment of Parkinson's Disease** *F1000Research* **9** https://doi.org/10.12688/F1000RESEARCH.25634.1

71. Sun H *et al.* (2021) **First-Time Disclosure of CVN424, a Potent and Selective GPR6 Inverse Agonist for the Treatment of Parkinson's Disease: Discovery, Pharmacological Validation, and Identification of a Clinical Candidate** *J Med Chem* **64** https://doi.org/10.1021/acs.jmedchem.0c02081

72. Torper O, Götz M, Jao C-W, Wu Y-T (2017) **Brain repair from intrinsic cell sources: Turning reactive glia into neurons** *Progress in Brain Research* https://doi.org/10.1016/bs.pbr.2016.12.010

73. Truong DJJ, Kühner K, Kühn R, Werfel S, Engelhardt S, Wurst W, Ortiz O (2015) **Development of an intein-mediated split-Cas9 system for gene therapy** *Nucleic Acids Res* https://doi.org/10.1093/nar/gkv601

74. Tsai SQ, Topkar V V., Joung JK, Aryee MJ (2016) **Open-source guideseq software for analysis of GUIDE-seq data** *Nat Biotechnol 2016 345* **34**:483–483 https://doi.org/10.1038/nbt.3534

75. Tsai SQ *et al.* (2014) **GUIDE-seq enables genome-wide profiling of off-target cleavage by CRISPR-Cas nucleases** *Nat Biotechnol 2014 332* **33**:187–197 https://doi.org/10.1038/nbt.3117

76. Valcárcel J, Gebauer F (1997) **Post-transcriptional regulation: The dawn of PTB** *Curr Biol* **7** https://doi.org/10.1016/s0960-9822(06)00361-7

77. Villiger L *et al.* (2018) **Treatment of a metabolic liver disease by in vivo genome base editing in adult mice** *Nat Med* https://doi.org/10.1038/s41591-018-0209-1

78. Wang LL, Serrano C, Zhong X, Ma S, Zou Y, Zhang CL (2021) **Revisiting astrocyte to neuron conversion with lineage tracing in vivo** *Cell* **184** https://doi.org/10.1016/j.cell.2021.09.005

79. Winter J, Luu A, Gapinske M, Manandhar S, Shirguppe S, Woods WS, Song JS, Perez-Pinera P (2019) **Targeted exon skipping with AAV-mediated split adenine base editors** *Cell Discov* **5** https://doi.org/10.1038/s41421-019-0109-7

80. Xue Y *et al.* (2013) **Direct conversion of fibroblasts to neurons by reprogramming PTB-regulated MicroRNA circuits** *Cell* https://doi.org/10.1016/j.cell.2012.11.045

81. Xue Y, Qian H, Hu J, Zhou B, Zhou Y, Hu X, Karakhanyan A, Pang Z, Fu XD (2016) **Sequential regulatory loops as key gatekeepers for neuronal reprogramming in human cells** *Nat Neurosci* **196**:807–815 https://doi.org/10.1038/nn.4297

82. Yang G, Yan Z, Wu X, Zhang M, Xu C, Shi L, Yang H, Fang K (2023) **Ptbp1 knockdown failed to induce astrocytes to neurons in vivo** *Gene Ther* **2023**:1–6 https://doi.org/10.1038/s41434-023-00382-5

83. Yu GL, Zhang Y, Ning B (2021) **Reactive Astrocytes in Central Nervous System Injury: Subgroup and Potential Therapy** *Front Cell Neurosci* https://doi.org/10.3389/fncel.2021.792764

84. Yu X, Nagai J, Khakh BS (2020) **Improved tools to study astrocytes** *Nat Rev Neurosci* https://doi.org/10.1038/s41583-020-0264-8

85. Zheng S, Gray EE, Chawla G, Porse BT, O'Dell TJ, Black DL (2012) **Psd-95 is post-transcriptionally repressed during early neural development by PTBP1 and PTBP2** *Nat Neurosci* **15** https://doi.org/10.1038/NN.3026

86. Zhou H *et al.* (2020) **Glia-to-Neuron Conversion by CRISPR-CasRx Alleviates Symptoms of Neurological Disease in Mice** *Cell* https://doi.org/10.1016/j.cell.2020.03.024

Author information

Desirée Böck[#]
Institute of Pharmacology and Toxicology, University of Zurich, Zürich, Switzerland
ORCID iD: 0000-0001-8142-0629

For correspondence: desiree.boeck@uzh.ch
[#]These authors contributed equally

Maria Wilhelm[#]
Institute of Pharmacology and Toxicology, University of Zurich, Zürich, Switzerland

[#]These authors contributed equally

Jonas Mumenthaler
Institute of Pharmacology and Toxicology, University of Zurich, Zürich, Switzerland

Daniel Fabio Carpanese
Institute of Pharmacology and Toxicology, University of Zurich, Zürich, Switzerland

Peter I Kulcsár
Institute of Pharmacology and Toxicology, University of Zurich, Zürich, Switzerland

Simon d'Aquin
Institute of Pharmacology and Toxicology, University of Zurich, Zürich, Switzerland

Alessio Cremonesi
Division of Clinical Chemistry and Biochemistry, University Children's Hospital Zurich, University of Zurich, Zurich, Switzerland

Anahita Rassi
Division of Clinical Chemistry and Biochemistry, University Children's Hospital Zurich, University of Zurich, Zurich, Switzerland

Johannes Häberle
Division of Metabolism and Children's Research Center, University Children's Hospital Zurich, Zurich, Switzerland

Tommaso Patriarchi
Institute of Pharmacology and Toxicology, University of Zurich, Zürich, Switzerland, Neuroscience Center Zurich, University of Zurich and ETH Zurich, Zurich, Switzerland
ORCID iD: 0000-0001-9351-3734

For correspondence: patriarchi@pharma.uzh.ch

Gerald Schwank
Institute of Pharmacology and Toxicology, University of Zurich, Zürich, Switzerland
ORCID iD: 0000-0003-0767-2953

For correspondence: schwank@pharma.uzh.ch

Editors

Reviewer #2 (Public review):

Summary:

The manuscript by Bock and colleagues describes generation of an AAV-delivered adenine base editing strategy to knockdown PTBP1 and the behavioral and neurorestorative effects of specifically knocking down striatal or nigral PTBP1 in astrocytes or neurons in a mouse model of Parkinson disease. The authors found that knocking down PTBP1 in neurons, but not astrocytes, and in striatum, but not nigra, results in the phenotypic reorganization of neurons to TH+ cells sufficient to rescue motor phenotypes, though insufficient to normalize responses to dopaminomimetic drugs.

Strengths:

The manuscript is well-written and adds to the growing literature challenging previous findings by Qian et al., 2020 and Zhou et al., 2020 indicating that astrocytic downregulation of PTBP1 can induce conversion to dopaminergic neurons in the midbrain and improve parkinsonian symptoms. The base editing approach is interesting and potentially more therapeutically relevant than previous approaches.

Weaknesses:

The animal model utilized, the 6-OHDA model, though useful to examine dopaminergic cell loss, exhibits accelerated neurodegeneration and none of the typical pathological hallmarks (synucleinopathy, Lewy bodies, etc.) compared to the typical etiology of Parkinson disease, limiting its translational interpretation. The identity of the converted neurons is unclear. Though the immunohistochemical methodology indicates they may be MSNs and/or interneurons, a more comprehensive identity is still lacking. There remains no real evidence that these cells actually release dopamine. Since striatal dopamine was assessed by whole-tissue analysis, which is not necessarily reflective of synaptic dopamine availability, it is difficult to assess whether the ~10% increase in TH+ cells in the striatum was sufficient to improve dopamine function. However, the improvement in motor activity suggests that it was.

https://doi.org/10.7554/eLife.97180.2.sa2

Reviewer #3 (Public review):

This study explores the use of an adenine base editing strategy to knock down PTBP1 in astrocytes and neurons of a Parkinson's disease mouse model, as a potential AAV-BE therapy. The results indicate that editing Ptbp1 in neurons, but not astrocytes, leads to the formation of tyrosine hydroxylase (TH)+ cells, rescuing some motor symptoms.

Several aspects of the manuscript stand out positively. Firstly, the clarity of the presentation. The authors communicate their ideas and findings in a clear and understandable manner, making it easier for readers to follow.

The Materials and Methods section is well-elaborated, providing sufficient detail for reproducibility.

The logical flow of the manuscript makes sense, with each section building upon the previous one coherently.

The ABE strategy employed by the authors appears sound, and the manuscript presents a coherent and well-supported argument.

Positively, some of the data in this study effectively counteracts previous work in line with more recent publications, demonstrating the authors' ability to contribute to the ongoing conversation in the field.

Comments on revisions:

The authors have adequately addressed all the previous questions and suggestions by providing new data and/or adding necessary clarifications and deeper discussions. The newly presented data convincingly fills the gaps identified during the initial review process. The additional discussions and clarifications enhance both the clarity and transparency of the manuscript.

https://doi.org/10.7554/eLife.97180.2.sa1

Author response:

The following is the authors' response to the original reviews.

> ***Public Reviews:***
>
> ***Reviewer #1 (Public Review):***
>
> *Summary:*
>
> *Recent years have seen spectacular and controversial claims that loss of function of the RNA splicing factor Ptbp1 can efficiently reprogram astrocytes into functional neurons that can rescue motor defects seen in 6-hydroxydopamine (6-OHDA)-induced mouse models of Parkinson's disease (PD). This latest study is one of a series that fails to reproduce these observations, but remarkably also reports that neuronal-specific loss of function of Ptbp1 both induces expression of dopaminergic neuronal markers in striatal neurons and rescues motor defects seen in 6-OHDA-treated mice. The claims, if replicated, are remarkable and identify a straightforward and potentially translationally relevant mechanism for treating motor defects seen in PD models. However, while the reported behavioral effects are strong and were collected without sample exclusion, other claims made here are less convincing. In particular, no evidence that Ptbp1 loss of function actually occurs in striatal neurons is provided, and the immunostaining data*

> *used to claim that dopaminergic markers are induced in striatal neurons is not convincing. Furthermore, no characterization of the molecular identity of Ptbp1-deficient striatal neurons is provided using single-cell RNA-Seq or spatial transcriptomics, making it difficult to conclude that these cells are indeed adopting a dopaminergic phenotype.*
>
> *Overall, while the claims of behavioral rescue of 6-OHDA-treated mice appear compelling, it is essential that these be independently replicated as soon as possible before further studies on this topic are carried out. Insights into the molecular mechanisms by which neuronalspecific loss of function of Ptbp1 induces behavioral rescue are lacking, however. Moreover, the claims of induction of neuronal identity in striatal neurons by Ptbp1 require considerable additional work to be convincing.*

We thank the reviewer for the detailed analysis of our study. Please find our answers to the points raised by the reviewer below in blue.

> *Strengths of the study:*
>
> *(1) The effect size of the behavioral rescue in the stepping and cylinder tests is strong and significant, essentially restoring 6-OHDA-lesioned mice to control levels.*
>
> *(2) Since the neurotoxic effects of 6-OHDA treatment are highly variable, the fact that all behavioral data was collected blinded and that no samples were excluded from analysis increases confidence in the accuracy of the results reported here.*

We appreciate the reviewer's feedback and acknowledgement of the strengths of our study. We undertook several optimization steps in the surgery, post-operative care, and handling of the animals for behavior experiments to ensure high reproducibility of our experiments.

> *Weaknesses of the study:*
>
> *(1) Neurons express relatively little Ptbp1. Indeed, cellular expression levels as measured by scRNA-Seq are substantially below those of astrocytes and other non-neuronal cell types, and Ptbp1 immunoreactivity has not been observed in either striatal or midbrain neurons (e.g. Hoang, et al. Nature 2023). This raises the question of whether any recovery of Th expression is indeed mediated by the loss of function of Ptbp1 rather than by off-target effects. AAVmediated rescue of Ptbp1 expression could help clarify this.*

In the original manuscript, we delivered control vectors that only express the ABE to 6-OHDAlesioned mice (labeled as AAV-ctrl) and did not detect TH positive cells in the midbrain or striatum of control mice or rescue of spontaneous motor skills. We can therefore exclude that the delivery procedure, AAV-PHP.eB capsid, or ABE expression caused adverse effects leading to induction of TH expression and functional rescue of spontaneous motor behaviors in PD mice. To further exclude that these effects were caused by off-target editing, we experimentally determined off-target binding sites of our sgRNA (sgRNA-ex3) using GUIDEseq and subsequently analyzed these sites in treated animals by NGS (Figure 3 – supplement 3). While two off-target sites were identified, it is unlikely that base editing at these sites caused the observed phenotypes. One off-target site was identified in the myopalladin (Mypn) gene, which encodes for a muscle-specific protein that plays a role in regulating the structure and growth of skeletal and cardiac muscle (Filomena et al., 2021, 2020). The other site is not located in a coding region, but in an intron of the ankyrin-1 (Ank1) gene, encoding for an adaptor protein linking membrane proteins to the underlying cytoskeleton (Cunha and Mohler, 2009). Even though this gene is also expressed in neurons, base editing within this intronic region did not lead to changes in transcript levels (Figure 3 – supplement 3). Thus, the induction of TH expression upon adenine base editing with sgRNA-ex3 is likely a direct consequence of PTBP1 downregulation.

Further supporting this conclusion, in the revised manuscript we additionally show PTBP1 downregulation at the RNA and protein level in the SNc and striatum after base editor treatment (Figure 2 – figure supplement 5; figure 3 – supplement 2).

> *(2) It is not clear why dopaminergic neurons, which are not normally found in the striatum, are observed following Ptbp1 knockout. This is very similar to the now-debunked claims made in Zhou, et al. Cell 2020, but here performed using the hSyn rather than GFAP mini promoter to control AAV expression. While this is the most dramatic and potentially translationally relevant claim of the study, this claim is extremely surprising and lacks any clear mechanistic explanation for why it might happen in the first place.*

We agree with the reviewer that our study does not provide mechanistic insights into how Ptbp1 downregulation in neurons leads to the induction of dopaminergic markers in the striatum. As we believe that this is not within the scope of a revision, we discuss potential follow-up experiments in the discussion section of the revised manuscript.

> *This observation is even more surprising in light of reports that antisense oligonucleotidemediated knockdown of Ptbp1, which should have affected both neuronal and glial Ptbp1 expression, failed to induce expression of dopaminergic neuronal markers in the striatum (Chen, et al. eLife 2022). Selective loss of function of Ptbp1 in striatal and midbrain astrocytes likewise results in only modest changes in gene expression.*

Using 6-OHDA lesioned *Aldh1l1-CreERT2;Rpl22lsl-HA* mice, the Chen et al. study (eLife 2022) assessed potential astrocyte to neuron conversion by quantifying the presence of HA-labeled neurons after ASO-mediated knockdown of Ptbp1. Even though they did not detect HApositive neurons in the SNc, suggesting absence of astrocyte to neuron conversion, the images in Figure 4D reveal TH positive cells in the lesioned hemisphere, similar to our observations in Figure 2B-D. While it cannot be excluded that these TH positive cells are remnants from an incomplete 6-OHDA lesion, they could also be endogenous neurons with induced expression of dopaminergic markers after ASO-mediated knockdown of Ptbp1. Furthermore, Chen et al. performed the apomorphine test to assess changes in motor skills, which did not reveal an improvement in our study either.

> *It is critically important that this claim be independently replicated, and that additional data be provided to conclusively show that striatal neurons are indeed expressing dopaminergic markers.*

Our behavior and immunofluorescence experiments involving mice injected into the striatum were performed with two independently generated cohorts of 6-OHDA mice. In detail, the 6OHDA mice were generated by two independent surgeons from different labs (>6 months between experiments of these cohorts), leading to comparable behavioral outcomes before and after treatment. Subsequent behavior and immunofluorescence experiments with each cohort were performed and analyzed by two independent and blinded researchers, showing comparable results.

> *(3) More generally, since multiple spectacular and irreproducible claims of single-step glial-toneuron reprogramming have appeared in high-profile journals in recent years, a consensus has emerged that it is essential to comprehensively characterize the identity of "transformed" cells using either single-cell RNA-Seq or spatial transcriptomics (e.g. Qian, et al. FEBS J 2021; Wang and Zhang, Dev Neurobiol 2022). These concerns apply equally*

> *to claims of neuronal subtype conversion such as those advanced here, and it is essential to provide these same datasets.*

In the revised version, we have analyzed the expression of additional neuronal markers in TH positive cells of the striatum using 4i imaging. Briefly, our results showed that the vast majority of TH-expressing cells also expressed the markers DAT and NEUN, further corroborating the neuronal and dopaminergic identity of these cells. Additional analysis revealed that this TH/DAT/NEUN expressing cell population expressed markers of GABAergic neurons, either of medium spiny neurons (~50%) and various types of interneurons (~50%). While our 4i analysis has allowed us to broadly classify these TH-expressing populations, we agree that detailed transcriptional analysis at the single cell level is required to understand the molecular mechanisms underlying the generation of TH positive cells. These analyses are, however, not within the scope of a revision and would require a thorough dedicated study. We have added these results and discussion points to the revised manuscript.

> *(4) Low-power images are generally lacking for immunohistochemical data shown in Figures 3 and 4, which makes interpretation difficult. DAPI images in Figure 3C do not appear nuclear. Immunostaining for Th, DAT, and Dcx in Figure 4 shows a high background and is difficult to interpret.*

We thank the reviewer for closely evaluating these images and suggestions for improvement. In the revised manuscript, we provide low power images and higher magnification insets as requested to allow for easier interpretation.

> *(5) Insights into the mechanism by which neuronal-specific loss of Ptbp1 function induces either functional recovery, or dopaminergic markers in striatal neurons, is lacking.*

In the revised manuscript, we provide a more detailed discussion of mechanisms that could potentially be involved in the functional recovery or expression of dopaminergic markers. However, deciphering the exact molecular mechanisms underlying these observations requires thorough transcriptional analysis at the single cell level, which is out of scope of this revision.

> ***Reviewer #2 (Public Review)**:*
>
> *Summary:*
>
> *The manuscript by Bock and colleagues describes the generation of an AAV-delivered adenine base editing strategy to knockdown PTBP1 and the behavioral and neurorestorative effects of specifically knocking down striatal or nigral PTBP1 in astrocytes or neurons in a mouse model of Parkinson's disease. The authors found that knocking down PTBP1 in neurons, but not astrocytes, and in striatum, but not nigra, results in the phenotypic reorganization of neurons to TH+ cells sufficient to rescue motor phenotypes, though insufficient to normalize responses to dopaminomimetic drugs.*
>
> *Strengths:*
>
> *The manuscript is generally well-written and adds to the growing literature challenging previous findings by Qian et al., 2020 and Zhou et al., 2020 indicating that astrocytic downregulation of PTBP1 can induce conversion to dopaminergic neurons in the midbrain and improve parkinsonian symptoms. The base editing approach is interesting and potentially more therapeutically relevant than previous approaches.*
>
> *Weaknesses:*

> *The manuscript has several weaknesses in approach and interpretation. In terms of approach, the animal model utilized, the 6-OHDA model, though useful to examine dopaminergic cell loss, exhibits accelerated neurodegeneration and none of the typical pathological hallmarks (synucleinopathy, Lewy bodies, etc.) compared to the typical etiology of Parkinson's disease, limiting its translational interpretation.*

We thank the reviewer for the detailed assessment of our study and pinpointing its current weaknesses. Please find our answers to all comments below in blue.

We agree with the reviewer that the 6-OHDA model lacks the typical pathological hallmarks of PD. Nevertheless, we chose this model for two reasons:

i) The 6-OHDA model was used by both Qian et al. (2020) and Zhou et al. (2020). To allow comparison of our results to these studies, it was crucial to use the same model. Notably, the 6-OHDA model was also used by Chen et al. (2022) and Hoang et al. (2023) for comparison to the two studies from 2020.

ii) The 6-OHDA model is straightforward to generate and displays robust motor impairments for evaluation of potential therapeutic effects of neuroregeneration treatment approaches. We therefore believe that the model is well-suited to analyze the cellular and behavioral effects (specifically motor skills) of PTBP1 downregulation.

In future studies, it would be critical to include models that also display typical pathological hallmarks of the disease to further evaluate the therapeutic effect of this base editing approach. These experiments are, however, not within the scope of this study, which was aimed to focus on the cellular and behavioral effects of PTBP1 downregulation.

> *In addition, there is no confirmation of a neuronal or astrocytic knockdown of PTBP1 in vivo; all base editing validation experiments were completed in cell lines.*

In the revised manuscript, we assess *in vivo* base editing efficiencies at the *Ptbp1* target site in the SNc (AAV-hsyn, 15.6%) and striatum (AAV-hysn, 21.1%). Furthermore, we assessed *in vivo Ptbp1* downregulation at the RNA and protein level to complement our *in vitro* data (Figure 2 – figure supplement 5; figure 3 – supplement 2).

> *Finally, it is unclear why the base editing approach was used to induce loss-of-function rather than a cell-type specific knockout, if the goal is to assess the effects of PTBP1 loss in specific neurons.*

We expressed base editors under cell-type specific promoter to induce a reliable loss-offunction mutation at the *Ptbp1* exon-intron junction in neurons or astrocytes. Performing these mutations with Cas9 nucleases instead would have had potential limitations and risks, including i) indel mutations do not always lead to a frameshift and loss-of-function despite high indel formation at the targeted site, ii) nucleases induce DNA double strand breaks, which can have serious side effects (e.g. chromosomal rearrangements or translocations), and iii) 'mosaicisms' as edited cells contain different indel mutations, which may result in different effects and thus complicate analysis of the downstream effects. We discuss these points in the revised manuscript.

> *In terms of interpretation, the conclusion by the authors that PTBP1 knockdown has little likelihood to be therapeutically relevant seems overstated, particularly since they did observe a beneficial effect on motor behavior. We know that in PD, patients often display negligible symptoms until 50-70% of dopaminergic input to the striatum is lost, due to compensatory activity of remaining dopaminergic cells. Presumably, a small recovery of dopaminergic neurons would have an outsized effect on motor ability and may improve*

> *the efficacy of dopaminergic drugs, particularly levodopa, at lower doses, averting many problematic side effects. Since striatal dopamine was assessed by whole-tissue analysis, which is not necessarily reflective of synaptic dopamine availability, it is difficult to assess whether the ~10% increase in TH+ cells in the striatum was sufficient to improve dopamine function. However, the improvement in motor activity suggests that it was.*

As pointed out by the reviewer, it is difficult to estimate the therapeutic effect and importance of a ~10% increase in TH+ cells for PD patient. Guided by the reviewer's suggestion, we have included a more in-depth discussion of our results and its potential therapeutic value as well as outstanding questions for future studies in the revised manuscript.

> ***Reviewer #3 (Public Review):***
>
> *This study explores the use of an adenine base editing strategy to knock down PTBP1 in astrocytes and neurons of a Parkinson's disease mouse model, as a potential AAV-BE therapy. The results indicate that editing Ptbp1 in neurons, but not astrocytes, leads to the formation of tyrosine hydroxylase (TH)+ cells, rescuing some motor symptoms.*
>
> *Several aspects of the manuscript stand out positively. Firstly, the clarity of the presentation. The authors communicate their ideas and findings in a clear and understandable manner, making it easier for readers to follow.*
>
> *The Materials and methods section is well-elaborated, providing sufficient detail for reproducibility.*
>
> *The logical flow of the manuscript makes sense, with each section building upon the previous one coherently.*
>
> *The ABE strategy employed by the authors appears sound, and the manuscript presents a coherent and well-supported argument.*
>
> *Positively, some of the data in this study effectively counteracts previous work in line with more recent publications, demonstrating the authors' ability to contribute to the ongoing conversation in the field.*

We thank the reviewer for appreciating the effort we have put into this study. Please find below a point-by-point reply to the weaknesses raised by the reviewer.

> *However, while the in vitro data yields promising results, it may have been overly optimistic to assume that the efficiencies observed in dividing cells will directly translate to in vivo conditions. This consideration is important given the added complexities of vector optimization, different cell types targeted in vitro versus in vivo, as well as unknown intrinsic limitations of the base editing technology.*

We agree with the reviewer that *in vitro* base editing efficiencies might not directly translate to *in vivo* editing outcomes. We therefore assessed *in vivo* base editing efficiencies at the *Ptbp1* locus and PTBP1 downregulation in the striatum and midbrain. Our data revealed that *in vivo* base editing activity was lower than in our *in vitro* setting (*in vitro*: Figure 1; figure 1 – figure supplement 2; *in vivo*: figure 2 – figure supplement 5; figure 3 – supplement 2). However, we believe that these rates are slightly underestimated since we sequenced DNA isolated from the whole tissue (striatum or SNc) and not from purified astrocytes or neurons. Moreover, we could demonstrate that editing led to a reduction of *Ptbp1* transcript and PTBP1 protein level (Figure 2 – figure supplement 5; figure 3 – supplement 2).

> *In addition, certain aspects of the manuscript would benefit from a more in-depth and comprehensive discussion rather than being only briefly touched upon. Such a discussion would enhance the relevance of the obtained results and provide the foundation for improvement when using similar approaches.*

Following the reviewer's suggestion, we included a more in-depth discussion of our results in the revised manuscript.

> ***Recommendations for the authors:***
>
> ***Reviewing Editor (Recommendations for the Authors):***
>
> *A summary of key recommendations that might improve the eLife assessment in a subsequent submission are provided below, as a guide to help the authors focus on changes that might enhance the strength of evidence (e.g., from "incomplete" to "solid").*
>
> *(1) Provide further explanation of the mechanistic relationship between the downregulation of Ptbp1 and TH+ dopaminergic neuron reprogramming. Additional discussion of this topic should also be included.*
>
> *(2) Demonstrate proof of editing in the intended targeted cells in vitro and/or in vivo.*
>
> *(3) Show evidence of successful Base Editor delivery in vivo.*
>
> *(4) Perform a deeper characterization of TH+ cells in vivo and provide a more thorough discussion of the identity of the targeted cells. This may include an exploration of whether TH+ cells detected are TH+ interneurons and/or establish their identity based on transcriptomics or a similar approach.*
>
> *(5) Provide better-quality representative images supporting the quantitative data.*
>
> *(6) Please include full statistical reporting including exact p-values wherever possible alongside the summary statistics (test statistic and df) and 95% confidence intervals. These should be reported for all key questions and not only when the p-value is less than 0.05 in the main manuscript.*

In the revised manuscript, we provided 1) suggestions of the mechanistic relationship between Ptbp1 knockdown, dopamine synthesis, and the functional rescue of spontaneous behaviors, 2) proof of *in vivo* base editing and successful base editor delivery, 3) deeper characterization of TH-expressing cells *in vivo* using 4i imaging, 4) better quality images, and 5) full statistical reporting.

> *Individual Reviewer recommendations for the authors are included below.*
>
> ***Reviewer #1 (Recommendations For The Authors):***
>
> *Confirm loss of Ptbp1 function in infected striatal neurons. Single-cell RNA-Seq or spatial transcriptomic analysis must be performed to characterize the identity of the edited striatal neurons. The quality of the immunostaining in Figures 3 and 4 needs to be improved, and lowpower images provided. Were eLife a conventional journal, I would have insisted on all these being included prior to publication. Please also arrange for independent replication of the behavioral rescue and induction of dopaminergic marker gene expression in the striatum.*

In the revised manuscript, we confirmed *Ptbp1* downregulation at the tissue level in the SNc and striatum by RT-qPCR and western blot and included low-power images for easier

interpretation. Additionally, we assessed expression of additional neuronal markers on striatal sections using 4i imaging and found that TH/DAT/NEUN positive populations either expressed markers of medium spiny neurons or interneurons. We have included these results in the revised manuscript.

Our behavioral and imaging experiments involving mice injected into the striatum were in fact performed with two independently generated cohorts of 6-OHDA mice. In detail, the 6OHDA mice were generated by two independent surgeons from different labs (>6 months between experiments of these two cohorts), leading to comparable behavioral outcomes before and after treatment. The experiments with each cohort were performed and analyzed by two independent and blinded researchers, yielding comparable results.

> ***Reviewer #2 (Recommendations For The Authors):***
>
> *(1) In the introduction, lines 43-45: This statement is inaccurate. Current treatment strategies do not focus on slowing or halting disease progression. There is currently no accepted therapy that does this. Dopaminergic therapies and deep brain stimulation can compensate for circuitry dysfunction as a result of dopamine cell loss but do not slow the disease. The referenced paper used is older and does not refer to new treatments for PD and is a summary article for a special issue of the Disease Models and Mechanisms journal. Please ensure that all references used are appropriate for the statement they are attached to.*

We thank the reviewer for pointing this out. We have rephrased this statement accordingly and provided an appropriate reference describing current treatment strategies.

> *(2) The number of TH+ cells in the intact nigra seems low compared to published data. Suggest a stereological approach may be better than the Abercrombie method.*

Following the reviewer's suggestion, we re-quantified the number of TH positive cells using a stereological approach (Nv:Vref method). We have included these results in the revised manuscript.

> *(3) Have the authors considered that the striatal TH+ cells could be TH+ striatal interneurons?*

In the revised manuscript, we performed additional 4i imaging experiments to further analyze the identity of the TH positive cells in the striatum. Briefly, we found that TH/DAT/NEUN positive populations either expressed markers of GABAergic medium spiny neurons or interneurons. We have added these results to the revised manuscript (Figure 4).

> *(4) The Western blot shown in Figure 1 C for C8-D1A has some abnormalities and makes it difficult to judge the bands. Also, for 1B, the legends are difficult to see.*

In the revised manuscript, we have repeated the respective western blot to make interpretation of the bands easier, and adapted the legends in Figure 1B for better visibility.

> *(5) Figure 2: Please show representative images for the GFAP-targeted editing.*

Representative images of the GFAP-targeted groups can be found in Figure 2 – figure supplement 3.

> *(6) Figure 2, Supplement 3: Please include quantification.*

The quantifications for these images can be found in Figure 2D and 2F.

> *(7) Figure 1, Supplement 2: The gene name in A is misspelled.*

Thank you for point this out. In the revised manuscript, we added the correct gene name.

> *(8) Line 267-276: As previously indicated, the statement here is overstated based on the data provided. In addition, the citation provided to justify this claim (Kannari et al., 2000) is an odd choice as the dosage of L-DOPA utilized was not therapeutically relevant (50 mg/kg). A better indication of efficacy would be the return to basal, unaffected levels rather than the fold increase in dopamine levels. A better comparison would be Lindgren et al., 2010 who showed that L-DOPA-treated animals with a physiologically relevant dose (6 mg/kg) that did not induce dyskinesia, showed a return to basal, non-lesioned dopamine levels in the striatum after LDOPA by microdialysis. To really support this claim, the authors would need to use an approach that could measure synaptic dopamine availability, rather than whole-tissue dopamine levels, such as microdialysis, fiber photometry, or an equivalent.*

Following the reviewer's suggestions, we replaced this reference with Lindgren et al. (2010) and provide a more detailed interpretation of our results and remaining questions for future studies.

> ***Reviewer #3 (Recommendations For The Authors):***
>
> *Major and minor issues are discussed below by section.*
>
> *INTRODUCTION and AIM - Lines 36-73*
>
> *- The authors effectively contextualize the aim of their study by providing comprehensive background information on previous research regarding cell 'reprogramming' into dopaminergic neurons in the SNc. However, the introduction lacks contextualization of TH+ cells and PD. For readers who may not be well-versed in the Parkinson's field, understanding the importance of TH (Tyrosine Hydroxylase) may be challenging, since the term "TH+ cells" is mentioned only once by the end of the introduction (line 71), to then become a key element in the entire study.*
>
> *- Providing a brief explanation of the role of Tyrosine Hydroxylase in the synthesis of L-DOPA would facilitate the reader's comprehension of why the presence of TH+ cells following Base Editing treatment is relevant.*
>
> *- Further elaboration on the relationship between the downregulation of the general RNA binding protein, PTBP1, and the specific dopaminergic-related readout, TH, would improve coherence and strengthen the linkage between the introductory section and the results.*

We thank the reviewer for the constructive suggestions. In the introduction of the revised manuscript, we describe the meaning and importance of TH in the context of dopamine synthesis and PD. Likewise, we briefly outlined the importance of the PTBP1/nPTBP regulatory loops during neuronal differentiation and maturation.

> *RESULTS*
>
> *Result Section 1 - Line 75-109*
>
> *- Thorough screening of sgRNAs targeting splice junctions across the Ptbp1 gene in HEPA cells, shows the achievement of high levels of editing (80-90%) with sgRNA-ex3 and sgRNAex7.*

> *- The data also indicates that editing translates into significant reductions in ptbp1 expression, along with an increase in the expression of genes repressed by PTBP1.*
>
> *- Despite obtaining lower percentages of editing events in N2a neuroblastoma cells and the C8-D1A astroglial cell line, the differential expression levels of ptbp1 and the readout genes remain significant. However, the gRNA screening assay is performed in immortalized, dividing cells.*
>
> *- Providing proof that Adenosine Base Editing of Ptbp1 is successful in non-dividing cells (such as SNc and/or striatal primary neurons) would strengthen the case for the potential therapy in the intended cell type.*

Following the reviewer's comment, we show *in vivo* base editing rates in the SNc and striatum of treated PD mice in the revised manuscript (Figure 2 – figure supplement 5; figure 3 – supplement 2).

> *- Moreover, assessing the expression levels of tyrosine hydroxylase by qPCR after Ptbp1 base editing in vitro could help contextualize the use of TH+ detection as an in vivo readout and may help explain why the total number of TH+ cells is low after ABE treatment in vivo - as shown in following sections.*

In the revised manuscript, we now provide quantifications of *in vivo* base editing efficiencies in the SNc (~15%) and striatum (~20%). As expected from these lower *in vivo* base editing rates, downregulation of *Ptbp1* at the transcript and protein level was less pronounced compared to our *in vitro* experiments. It seems likely that higher base editing efficiency and more pronounced downregulation of *Ptbp1* could lead to a larger population of TH expressing cells. We have added these results and interpretations to the revised manuscript.

> *- Furthermore, although ABEs are less prone to generating bystander and other nucleotide changes compared to CBEs, it is still possible. Figures 1 (line 811) and 1-supplement 2 (line 842) only show a brief window of the Sanger sequencing trace. Updating these figures to display a wider view of the sequencing trace would enhance transparency. If unwanted edits are detected, while they may not significantly alter the relevance, impact, or structure of the paper, they may become an important aspect of the discussion.*

Indeed, ABEs can induce bystander edits and we also detected such edits at the *Ptbp1* target site. However, since our base editing strategy was designed to yield a loss of *Ptbp1* function, bystander editing at the splice site was not a primary focus in our analysis. Nevertheless, we included CRISPResso output images showing the specific editing outcomes in a wider analysis window in the revised manuscript (Figure 3 – figure supplement 2).

> *Result Section 2 - Lines 110-159*
>
> *A split intein system is used in vivo with sgRNA-ex3, after updating the promoter to make it cell-specific: hSyn to restrict expression to neurons and GFAP to restrict expression to astrocytes.*
>
> *However, no other assay is performed to assess whether a) the promoter change and/or b) splitting Cas9 may affect the editing efficiency compared to their initial in vitro approach.*

In the revised manuscript, we assessed the performance of the *in vivo* AAV vectors encoding the split intein ABE with sgRNA-ex3 *in vitro* in N2a and C8-D1A cells. Our results show that all vectors are functional and result in base editing at the target locus.

> *- Addressing whether this is the case may explain the low number of TH+ cells observed in vivo.*
>
> *- The authors could also consider staining for Cas9 to address whether the low number of TH+cells could be attributed to a poor Cas9 delivery.*

To confirm successful *in vivo* base editor delivery, we quantified *in vivo* base editing efficiencies in the SNc and striatum of PD mice. Our analysis revealed *in vivo* base editing efficiencies at both tissue sites, confirming that base editors were successfully delivered. Editing efficiencies were, however, substantially lower (Figure 2 – figure supplement 5; figure 3 – supplement 2). than in our *in vitro* cell line setting (Figure 1; figure 1 – figure supplement 2). Even though tissue editing rates likely underestimate the cell type-specific editing rates in astrocytes or neurons, higher base editing rates would have likely resulted in a higher number of TH positive cells. We have added these results and their implications to the revised manuscript.

> *- Moreover, despite the presence of TH, in Figure 2 E,F authors examine the striatal innervation from newly generated TH+ cells in the SNc by Fluorescence Intensity (FI) to conclude that the edited cells do not form projections towards the striatum. Considering the low levels of TH+ positive cells obtained, the accumulation of gross FI might not be the most accurate way to assess the presence or absence of cell projections.*
>
> *- Using another marker that stains the projections rather than the cell soma, and that is a marker of dopaminergic neurons, might be a better way to address this.*

To address the reviewer's comment, we analyzed the presence of potential dopaminergic fibers in the mfb, where projections are more concentrated (around the injection coordinates of 6-OHDA), using the dopaminergic marker DAT. In line with our previous observations in the striatum, we did not detect an increase in DAT fluorescence intensity upon treatment on the lesioned hemisphere (Figure 2 – figure supplement 4).

> *Result Section 3 - Line 160-182*
>
> *Minor issue*
>
> *- The same dual split intein system is used in the striatum. However, in Figure 3 - Figure Supplement 1 - line 958 and in Figure 3 - Figure Supplement 4 - line 1000authors show the injection of 2x the viral genomes indicated along the manuscript. In previous experiments the SNc 2x108vg/animal was used whereas this figure shows 4x108vg/animal injected in the striatum.*
>
> *- The authors should clarify if the vg injected in the striatum was different from what they previously indicated.*

Compared to injection in the SNc, the volume of vector injected in the striatum was doubled since the region is significantly larger. We clarified that the injected vector genomes were different between striatum and SNc in the revised manuscript.

> *Result Section 4- Line 183-220*
>
> *In this section, the authors thoroughly examine the neuronal nature of TH+ cells through NeuN co-staining and iterative immunofluorescence imaging (4i). BrdU experiments are conducted to determine the origin of these cells, leading to the conclusion that TH+ cells derive from nondividing cells and express the neuronal marker DAT, characteristic of dopamine-producing neurons (DANs). Cell shape of the TH+ cells in the striatum and SNc*

> *is also evaluated measuring their Feret's diameter and their cell surface. Authors conclude there's heterogeneity in the TH+ cell population due to the presence of TH+/Neun- as well as differences in cell shape.*
>
> *However, their explanation of this heterogeneity is solely attributed to differences in the microenvironment and lacks further elaboration. Similarly, their observation that almost half the number of TH+ striatal cells after treatment express CTIP2 (Line 213 and Figure 4B), a marker for GABAergic medium spiny neurons, which they state as "interesting" (line 213) is not developed further. Delving deeper into these topics could strengthen the discussion.*

In the revised manuscript, we provided a more in-depth discussion of the 4i imaging results and potential therapeutic implications. Additionally, we suggest follow-up experiments to analyze the identity, function, and molecular mechanisms underlying the expression of TH upon PTBP1 downregulation in future studies.

> *Result Section 5- Line 221-243*
>
> *Two drug-free and two drug-induced behavioral tests are conducted in control and treated animals to evaluate the restoration of motor functions following treatment. Consistent with their previous findings, only the treatment targeted to neurons resulted in the restoration of motor functions in drug-free behavioral tests. The rationale behind each test and its evaluation is clearly explained.*
>
> *DISCUSSION*
>
> *- In the discussion section, the authors effectively re-examine their results contextualizing their data with previous studies in the field. However, it would be helpful at this point in the manuscript to reconsider the use of the term 'cell reprogramming,' as this study does not involve actual cell reprogramming. The concept "reprograming" entails the process of transforming adult cells into a stem cell-like state, to then differentiate them into a different cell type. As proven in section 4 by a BrdU proliferation assay, the targeted cells are differentiated neurons. Considering BrdU is administered 5 days after ABE treatment, if true cell reprogramming was taking place, there should be evidence of BrdU incorporation. Cell reprogramming or reprograming is mentioned 4 times in the manuscript (line 34, line 54, line 265, line 277). Therefore, using another terminology would be more accurate.*

Following the reviewer's suggestion, we removed the term "cell reprograming" from the manuscript and rather describe it as induction of TH expression in endogenous neurons.

> *- As noted in the comments of section 4, a more thorough discussion about the various possibilities for heterogeneity would enhance the manuscript's contribution to the PD field.*

In the revised manuscript, we provided a more in-depth discussion of the 4i imaging results and potential therapeutic implications.

> *- Despite observing low numbers of TH+ cells, no significant rescue of drug-induced behaviors, and low levels of released dopamine, the authors merely state that these results make the therapy non-viable, but there is no further exploration or discussion. Whether the limitations lie in the ABE strategy itself, such as its efficiency in targeting and editing of differentiated neurons; or if the issues lie on the injection and delivery, is never discussed. A deeper argumentation on the possible underlying reasons for these*

> *challenges would greatly enhance the manuscript and contribute to the advancement of ABE therapies in the brain.*

We believe that the efficacy of our base editing approach could be significantly enhanced by optimizing the delivery. Currently, we are using a dual AAV approach to deliver intein-split ABEs. Since this approach relies on the delivery of higher AAV doses to achieve cotransduction of a cell by two different AAVs, the efficiency could be significantly enhanced by using smaller Cas9 orthologues that can be delivered as a single AAV. Furthermore, in this study we performed a single injection into the dorsal striatum to deliver ABE-expressing AAVs. Performing multiple injections into the rostral, medial, and caudal regions of the striatum might allow us to transduce more cells and induce TH expression in a larger population of striatal neurons. We have included these points in the revised manuscript.

> *- While drug-induced behaviors are not recovered, the data demonstrates a rescue of spontaneous behaviors. Further discussion on the potential differences in circuitry underlying these variations in behavioral rescue would also enrich the manuscript's discussion.*

In the revised manuscript, we provide suggestions for potential mechanisms involved in the rescue of spontaneous behavior vs. absence of rescue of drug-induced behaviors.

> *FIGURES AND FIGURE SUPPLEMENTS*
>
> *General minor issue - low magnification images in the following figures, make it difficult to visualize positive cells in tissue sections: Figure 2; Figure 2- supplement 1; Figure 2 - supplement 3, Figure 3- supplement 1. Adding a higher magnification imaging of positive cells in tissue sections of SNc and striatum might help with the visualization.*

As suggested by the reviewer, we included higher magnification images in the corresponding figures to improve interpretation of our results.

https://doi.org/10.7554/eLife.97180.2.sa0